JNeurosci
THE JOURNAL OF NEUROSCIENCE

Research Articles: Neurobiology of Disease

Repulsive guidance molecule a (RGMa) induces neuropathological and behavioral changes that closely resemble Parkinson's disease

J.a. Korecka[1], E. B. Moloney[1], R. Eggers[1], B. Hobo[1], S. Scheffer[1], N. Ras-Verloop[1], R.j. Pasterkamp[2], D.f. Swaab[3], A.b. Smit[4], R.e. Van Kesteren[4], K. Bossers[1] and J. Verhaagen[1,4]

[1]*Department of Regeneration of Sensorimotor Systems, Netherlands Institute for Neuroscience, An Institute of the Royal Netherlands Academy of Arts and Sciences, Meibergdreef 47, 1105 BA, Amsterdam, The Netherlands*

[2]*Department of Translational Neuroscience, Brain Center Rudolf Magnus, Utrecht University, Universiteitsweg 100, 3584 CG, Utrecht, The Netherlands*

[3]*Department of Neuropsychiatric Disorders, Netherlands Institute for Neuroscience, An Institute of the Royal Netherlands Academy of Arts and Sciences, Meibergdreef 47, 1105 BA, Amsterdam, The Netherlands*

[4]*Center for Neurogenomics and Cognitive Research, Neuroscience Campus Amsterdam, Vrije Universiteit Amsterdam, De Boelelaan 1085-1087, 1081 HV, The Netherlands*

DOI: 10.1523/JNEUROSCI.0084-17.2017

Received: 8 January 2017

Revised: 12 July 2017

Accepted: 11 August 2017

Published: 21 August 2017

Author contributions: JK- experimental design, experimental execution, acquiring data, analyzing data, writing the manuscript; EM- experimental execution, acquiring data, analyzing data, writing the manuscript; RE- experimental execution, experimental design; BH-experimental execution; SS- experimental execution, acquiring data, analyzing data; NRV- experimental execution, acquiring data, analyzing data; RP- experimental design, providing reagents; DS- experimental design,; AS- experimental design, ; RK- experimental design,; KB- experimental design, experimental execution, help with analyzing the data, writing the manuscript; JV- experimental design, writing the manuscript

Conflict of Interest: The authors declare no competing financial interests.

Corresponding author: Joanna A. Korecka, Current Address: Neuroregeneration Research Institute, McLean Hospital, MRC 1, 115 Mill Street, Belmont, MA 02478, USA, Telephone number: +1 617-855-2094, Email: jkorecka@mclean.harvard.edu,

Cite as: J. Neurosci ; 10.1523/JNEUROSCI.0084-17.2017

Repulsive guidance molecule a (RGMa) induces neuropathological and behavioral changes that closely resemble Parkinson's disease

Abbreviated title: RGMa induces degeneration of midbrain DA neurons

J.A. Korecka[1], E. B. Moloney[1], R. Eggers[1], B. Hobo[1], S. Scheffer[1], N. Ras-Verloop[1], R.J. Pasterkamp[2], D.F. Swaab[3], A.B. Smit[4], R.E. Van Kesteren[4], K. Bossers[1], J. Verhaagen[1, 4]

[1] Department of Regeneration of Sensorimotor Systems, Netherlands Institute for Neuroscience, An Institute of the Royal Netherlands Academy of Arts and Sciences, Meibergdreef 47, 1105 BA, Amsterdam, The Netherlands
[2] Department of Translational Neuroscience, Brain Center Rudolf Magnus, Utrecht University, Universiteitsweg 100, 3584 CG, Utrecht, The Netherlands
[3] Department of Neuropsychiatric Disorders, Netherlands Institute for Neuroscience, An Institute of the Royal Netherlands Academy of Arts and Sciences, Meibergdreef 47, 1105 BA, Amsterdam, The Netherlands
[4] Center for Neurogenomics and Cognitive Research, Neuroscience Campus Amsterdam, Vrije Universiteit Amsterdam, De Boelelaan 1085-1087, 1081 HV, The Netherlands

Corresponding author:

Joanna A. Korecka, *Current Address:* Neuroregeneration Research Institute, McLean Hospital, MRC 1, 115 Mill Street, Belmont, MA 02478, USA, Telephone number: +1 617-855-2094, Email: jkorecka@mclean.harvard.edu,

Abstract

Repulsive guidance molecule member a (RGMa) is a membrane-associated or released guidance molecule that is involved in axon guidance, cell patterning and cell survival. In our previous work we showed that RGMa is significantly upregulated in the substantia nigra of patients with Parkinson's disease. Here we demonstrate the expression of RGMa in midbrain human dopaminergic neurons. To investigate whether RGMa might model aspects of the neuropathology of Parkinson's disease in mouse, we targeted RGMa to adult midbrain dopaminergic neurons using adeno-associated viral vectors. Overexpression of RGMa resulted in a progressive movement disorder, including motor coordination and imbalance, which is typical for a loss of dopamine (DA) release in the striatum. In line with this, RGMa induced selective degeneration of dopaminergic neurons in the SN and affected the integrity of the nigrostriatal system. The degeneration of dopaminergic neurons was accompanied by a strong microglia and astrocyte activation. The behavioral, molecular and anatomical changes induced by RGMa in mice are remarkably similar to the clinical and neuropathological hallmarks of Parkinson's disease. Our data indicate that dysregulation of a repulsive axon guidance cue (RGMa) plays an important role in the pathology of Parkinson's disease and antibody-mediated functional interference with RGMa may be a disease modifying treatment option.

Significance statement

Parkinson's disease (PD) is a neurodegenerative disease characterized by severe motor dysfunction due to progressive degeneration of mesencephalic dopaminergic (DA) neurons in the substantia nigra (SN). To date there is no regenerative treatment available. We previously showed that repulsive guidance molecule member a (RGMa) is upregulated in the SN of PD patients. AAV-mediated targeting of RGMa to mouse DA neurons showed that overexpression of this repulsive axon guidance and cell patterning cue models the behavioral and neuropathological characteristics of PD in a remarkable way. These findings have implications for therapy development as interfering with the function of this specific axon guidance cue may be beneficial to the survival of DA neurons.

Introduction

Parkinson's disease (PD) is the second most prevalent neurodegenerative disease Patients suffer from motor (Dauer and Przedborski, 2003; Jankovic, 2008) and cognitive dysfunction (Jankovic, 2008; Olanow et al., 2009). The motor symptoms are mainly attributed to the loss of mesencephalic dopaminergic (DA) neurons in the substantia nigra (SN). The etiology of PD is multifactorial (Kalia and Lang, 2015), including both genetic (Kumaran and Cookson, 2015; Hernandez et al., 2016) and environmental components (Gorell et al., 2004). Transcriptional profiling (reviewed in Cooper-Knock et al., 2012), and pathway analysis (Lesnick et al., 2007; Lin et al., 2009; Srinivasan et al., 2009; Sutherland et al., 2009; Edwards et al., 2011) have revealed dysregulation of genes involved in processes previously implicated in PD (the ubiquitin/proteasome system, heat shock regulation, iron and vesicular transport, neurotransmission, oxidative stress), however also implicated novel pathways in PD, including axon guidance, extracellular matrix, polyamine signaling and microRNA modulation of mitochondrial function (Minones-Moyano et al., 2011).

Repulsive guidance molecule a (RGMa) is upregulated in DA neurons of PD patients (Bossers et al., 2009; Biosciences, 2012) suggesting a link between RGMa and PD. RGMa has also been implicated in other neurodegenerative diseases. It's increased expression contributes to the repulsive environment of the neural scar (Schwab et al., 2005a; Schwab et al., 2005b; Hata et al., 2006; Mueller et al., 2006; Yamashita et al., 2007) and a chromosome microdeletion in the RGMa gene has been linked to Angelman syndrome (Capelli et al., 2012). RGMa is also implicated in multiple sclerosis (MS) (Nohra et al., 2010; Muramatsu et al., 2011; Kubo et al., 2012; Tanabe and Yamashita, 2014; Demicheva et al., 2015) where RGMa-antibodies increased axonal outgrowth, ameliorated remyelination and improved function in a rodent MS-model (Muramatsu et al., 2011; Kubo et al., 2012; Tanabe and Yamashita, 2014).

RGMa acts as a repulsive axon guidance molecule in the developing amphibian, bird and mammalian brain (Monnier et al., 2002; Niederkofler et al., 2004; Samad et al., 2004; Matsunaga et al., 2006; Mueller et al., 2006; Yamashita et al., 2007). RGMa is processed by extracellular proteases to generate membrane-bound and soluble forms, which function as short- and a long-range guidance cues (Tassew et al., 2012) by interacting with its receptor neogenin (Yamashita et al., 2007). Many

embryonic neurons are sensitive to RGMa-neogenin repulsive signaling (Monnier et al., 2002; Conrad et al., 2007; Metzger et al., 2007; Kubo et al., 2008; Yoshida et al., 2008; Tassew et al., 2012). Neogenin is expressed by developing DA neurons (van den Heuvel et al., 2013) and continues to be expressed by adult neurons in the brain (Rodriguez et al., 2007).

RGMa-neogenin signaling also plays a role in neuronal survival, proliferation and differentiation (Matsunaga and Chedotal, 2004; Matsunaga et al., 2004; Matsunaga et al., 2006; Cole et al., 2007; Metzger et al., 2007; Lah and Key, 2012). Administration of RGMa promotes retinal ganglion cell survival after an optic nerve lesion (Koeberle et al., 2010) and improves neuronal survival following stroke (Paxinos, 2001). The pro-survival signaling of RGMa-neogenin is dependent on the interaction of neogenin with lipid rafts (Shabanzadeh et al., 2015).

Since RGMa is upregulated in the SN of human PD brains (Bossers et al., 2009; Biosciences, 2012), has deleterious effects in other disorders such as MS, and has a well-documented role in axon repulsion (Monnier et al., 2002; Niederkofler et al., 2004; Samad et al., 2004; Matsunaga et al., 2006; Mueller et al., 2006; Yamashita et al., 2007), we hypothesized that overexpression of RGMa in the mouse SN would negatively impact the midbrain dopaminergic system. We show that neuronal overexpression of RGMa induced a movement disorder typical for loss of striatal DA, degeneration of DA neurons in the SN, loss of DA nigrostriatal axonal projections, and microglial and astrocyte activation. These data indicate that RGMa is a negative regulator of DA neuron survival and may play an important role in PD pathology.

Materials and Methods

Human brain tissue samples

Brain tissue used in these studies was from the same controls and PD patients as described in Bossers et al. (2009). In brief, formalin-fixed, paraffin-embedded post-mortem human substantia nigra (SN) tissue from 7 PD patients and 9 controls was obtained from the Netherlands Brain Bank (NBB, Amsterdam, the Netherlands). Table 1 summarizes their clinico-pathological data.

In situ hybridization on human brain tissue samples

For semi-quantitative analysis of mRNA expression, one SN section from every subject was used (Table 1). The sections were deparaffinized, rehydrated and heated in a microwave in 0.1M citrate buffer pH 6.0 for 20 minutes. Sections were washed two times in PBS for 5 min, deproteinated for 20 mins in 0.2 N HCl, washed twice for 5 min in PBS, and treated with proteinase K (10ug/ml, Invitrogen) in proteinase K buffer (2 mM CaCl2, 10 mM Tris-HCl, pH 7.5) for 15 minutes at 37^0C. The proteinase K digestion was stopped by a 30 min incubation in glycin buffer (27mM glycine in PBS) followed by two 5 min washes in phosphate buffered saline (PBS). Finally, sections were delipidated for 10 min in PBS- 0.1% Triton X-100 (Sigma-Aldrich) and washed twice for 5min in PBS.

An RGMA-specific LNA-2'Omethyl-RNA modified oligonucleotide probe 5'-FAM-TugAccAcuTccTcuGgcA-3', recognizing nucleotides 1169-1187 of the human RGMa mRNA (NM_020211.2), was obtained from RiboTask Aps (Denmark). Sections were prehybridized overnight at room temperature (RT) in 200µl LNA hybridization buffer (50% formamide, 600mM NaCl, 10mM Hepes buffer pH7.5, 5x Denhardt's, 1mM EDTA, 200 µg/ml denatured herring sperm DNA). Next, the probe was diluted in LNA hybridization buffer to a concentration of 25nM, denatured at 95^oC for 5 min and cooled on ice for 5 min. Sections were hybridized in this buffer at 55^oC for 90 min, followed by a series of wash steps: 5 min in 5x SSC at 55^oC, 5 min in 2x SSC at 55^oC, 5 min in 0.2x SSC at 55^oC and 5 min in PBS at RT. To detect the probes, sections were pre-incubated with 1% milk-tris buffered saline (TBS) pH 7.6 for 1h, followed by 3 h incubation with sheep IgG, anti-fluorescein-AP-Fab fragments (Roche) diluted 1:3000 in 1% milk-Super Mix all at RT.

The hybridization signal was developed as follows. Sections were washed twice in Buffer 1 (100mM Tris, 150mM NaCl, pH7.5) and once in Buffer 2 (100mM Tris-HCl pH 9.0, 100mM NaCl, 5mM $MgCl_2$) for 5 min and further incubated in 10 ml Buffer 2 containing 3.4 mg nitro-blue tetrazolium chloride (Roche), 1.75 mg 5-bromo-4-chloro-3'-indolyphosphate p-toluidine salt (Roche) and 2.4 mg levamisole (Sigma-Aldrich) for 25 minutes. Reaction was stopped in water and slides were treated with 100% methanol for 5 min and cover slipped with aquamount (Merck). An adjacent section was incubated with sense probe to test the specificity of the observed *in situ* hybridization signal.

Immunohistochemistry on human post-mortem brain tissue

For protein localization, one SN section was used from each PD and control sample. The sections were deparaffinized in xylene, rehydrated in a graded series of ethanol and washed twice for 2 min in distilled water. Antigen retrieval was performed by microwave heating (2x 5 min at 700W) in 50mM Tris-HCl pH 9.0 and sections were washed in TBS twice for 5 min. Sections were blocked with TBS-0.1% Milk for 1 hour at RT. Sections were then incubated with anti-RGMa antibody (SC-46482, Santa Cruz, 1:25, an antibody raised against a 15 to 25 amino acids peptide mapping within the region of amino acids 300 to 350 of C-terminal human RGMa) and either anti-tyrosine hydroxylase antibody (TH, Jacques Boy SA, Reims, France, 1:1000) or anti-Neogenin antibodies (SC-15337, Santa Cruz, 1:25) diluted in Super Mix-0.1% milk solution at pH 7.6 (1x TBS, 0.25% gelatin (Merck, New Jersey, USA) and 0.5% Triton X-100 (Sigma-Aldrich, St Louis, Missouri, USA)) for 1 hour at RT followed by overnight incubation at 4°C. After the primary antibody incubation, sections were washed three times with TBS. To enhance the staining potential for RGMa we first amplified the signal by applying a biotin-labeled secondary antibody (1:400; Vector Laboratories, Burlingame, CA, USA) diluted in SuperMix for 1h at RT to the sections. Sections were subsequently incubated in ABC solution (1:800 in TBS, Vector Laboratories) for 1h at RT followed by a second round of signal amplification with a biotinylated tyramine incubation for 10min in a TBS-0.01% H_2O_2 solution (1:750). Finally the sections were incubated for 2 hours at RT with a streptavidin-conjugated Alexa 594 antibody (1:800 in TBS, Invitrogen) and for TH and neogenin detection, an anti-rabbit Alexa 488 conjugated antibody (1:800 in TBS, Invitrogen). To quench autofluorescence, sections were treated with 0.5% filtered Sudan Black solution

(BDH, Poole, England) for 7 min, briefly washed in 70% ethanol and TBS. Sections were embedded in Mowiol (0.1 M Tris pH 8.5, 25% glycerol, 10% w/v Mowiol 4-88 (Sigma-Aldrich)) containing Hoechst 33258 (BioRad, Hercules, CA, USA; 1:10000). Images were acquired on the confocal laser scanning microscope (CLSM, Zeiss, Sliedrecht, The Netherlands).

AAV constructs and viral vector production

Plasmids pAAV2Sna-SW and pTRUF20B-SEW [generous gifts from Prof. Deniz Kirik (Lund University, Sweden)] formed the basis for the production of the AAV vectors used in this study. Each plasmid contained two inverted terminal repeats of AAV2 flanking a human synapsin 1 (SYN) promoter driving expression of either human α-synuclein (pAAV2Sna-SW plasmid) or GFP (pTRUF20B-SEW plasmid), followed by a woodchuck hepatitis *virus* post-transcriptional regulatory element (WPRE) and a polyadenylation signal. For the construction of the empty vector (pAAV2-SYN) the pAAV2Sna-SW plasmid was cut with BamHI to remove the α-synuclein sequence and religated. For the construction of the vector containing mouse RGMa (pAAV2-SYN-RGMa) plasmid pcDNA4/HisB-RGMaFL was cut with Dra1 and Xho1 to isolate the full length mouse RGMa sequence (NM_177740) and this fragment was ligated into the pAAV2Sna-SW cut with EcoRV and Xho1.

Production of AAV2/7-SYN-Empty, AAV2/7-SYN-RGMa and AAV2/7-SYN-GFP viral vectors was performed using capsid and helper plasmids provided by J.M. Wilson (Gao et al., 2002). For each viral vector stock eight 15 cm petridishes containing $1x10^7$ human embryonic kidney 293T (HEK293T) cells were transfected with the use of polyethylenimine (PEI, MW25000; Polysciences Inc., Warrington, PA, USA). Cells were grown in Dulbecco's modified Eagle's medium (DMEM) containing 10% fetal calf serum (FCS) and 1% penicillin/streptomycin (GIBCO-Invitrogen Corp, New York, NY, USA). pAAV2-SYN, pTRUF20B-SEW and pAAV2-SYN-RGMa plasmids were cotransfected with packaging plasmids in a 1:2:2 ratio (AAV-gene plasmid : helper plasmid pAdΔF6 : AAV2/7 capsid plasmid) with a total amount of 62.5µg of DNA per plate. Two days after transfection cells were harvested in Dulbecco's phosphate buffered saline (D-PBS containing Ca^{2+} and Mg; Gibco) containing 10µg/ml DNAseI (Roche Diagnostics GmbH, Mannheim, Germany) and incubated for 1 hour at 37°C. Cells were lysed by three freeze-thaw cycles, centrifuged for 30 min at 4000rpm and the crude lysate was collected. The virus was

purified by iodixanol gradient ultra-centrifugation (Hermens et al., 1999; Zolotukhin et al., 1999) diluted in D-PBS (with Ca^{2+} and Mg; Gibco) containing 5% sucrose and concentrated using an Amicon 100kDA MWCO Ultra-15 device (Millipore, Billerica, MA, USA). Viral vector stocks were aliquoted and stored at -80°C until use. Titers were determined by quantitative PCR on DNAse-treated viral particles using WPRE directed primers (forward: CAGGTGTATTGCCACAAGACAAA and reverse: TGCACAGGTGAAGACCAAGCAA). AAV-Empty viral vector gave a titer of $8.6x10^{12}$ genomic copies per milliliter (gc/ml), AAV-GFP viral vector gave a titer of $3.0x10^{12}$gc/ml and AAV-RGMa virus gave a titer of $9.7x10^{12}$ gc/ml. Virus was used in two experiments using either a low or a high titer dosage: $3.0x10^{12}$ gc/ml and $9.0x10^{12}$ gc/ml respectively (Table 2). For the low titer experiment, the AAV-Empty and AAV-RGMa viruses were diluted in D-PBS/5% sucrose accordingly to titer-match the AAV-GFP virus.

AAV vector validation by western blot analysis

N2A cells were plated in 24-well plates and transfected with pTRUF20B-SEW and pAAV2-SYN-RGMa plasmids one day after plating with the use of PEI. On day 6, media and cells were harvested. Cells were lysed on ice for 10 min in 70µl RIPA buffer (25mM Tris-HCl pH 7.4 (Sigma), 150mM NaCl (Sigma), 1% NP40 (AppliChemicals, Darmstadt, Germany), 1% sodium deoxycholate (Sigma), 0.1% SDS and Complete Protease Inhibitor (Roche)). The cell lysate was sonicated and its protein concentration determined using the bicinchoninic acid protein assay kit (Pierce, Thermo Scientific). For western blot analysis, each sample was heated in 5X loading buffer containing 10% sodium dodecyl sulphate (SDS, MP Biomedicals) and 5% ß-mercaptoethanol (Sigma) at 95°C for 5min and separated on an 10% polyacrylamine-SDS gel. Proteins were transferred to nitrocellulose membranes and treated with block mix (5% milk in 1XTBS/0.5% Triton X-100) for 1h at RT. Blots were incubated with goat anti-mouse RGMa antibody (1:100, R&D systems AF2458, an antibody raised against amino acids 48 to 421 of human RGMa) and ß-actin (1:1000, Sigma-Aldrich, A5316) at 4°C overnight in block mix. The primary antibodies were detected with anti-goat -Cy5 (1:800, Jackson's Lab) and anti-mouse IR-dye 800 conjugated antibodies (1:2000, Thermo Scientific). Blots were scanned using the Odyssey infrared imager and Odyssey 2.1 scanning software (LI-COR biosciences).

Experimental animals and surgical procedures

Male C57BL/6 mice weighing 20-25g (Harlan, Zeist, The Netherlands) were socially housed with food and water *ad libitum*, in 12 hour light and dark cycles. The experimental procedures and postoperative care were carried out in accordance with the Institutional Animal Care and Use Committee of the Royal Netherlands Academy of Arts and Sciences.

The viral vector injections were carried out with the use of glass capillaries (1.0mm external diameter) with an 80 µm tip diameter connected via Portex polyethylene tubing to a Hamilton syringe fixed in a micro-infusion pump (PHD2000, Harvard Apparatus, Holliston, MA, USA). Two experiments were performed with animals injected unilaterally (into the right SN) with a low titer ($3.0x10^{12}$ gc.ml) and uni- or bilaterally with a high titer ($8.7\text{-}9.0x10^{12}$ gc.ml) virus (Table 2).

Mice were intraperitoneally (IP) injected with a mix of Hypnorm (0.1 mg/kg Fentanyl citrate/ 3.3 mg/kg Fluanisone HCl, Janssen Pharmaceuticals) and Dormicum (8.3 mg/kg Midazolam, Roche) and placed into a stereotactic device (David Kopf Instruments, Tujunga, CA, USA). The skull was leveled using the heights of Bregma, Lambda and two lateral measurements 2.0 mm from Bregma. The injection coordinates from Bregma were -2.8 mm anterior posterior and +/-1.3 mm lateral and -4.3 mm ventral dorsal (VD) from the dura. Subsequently, the needle was lowered into the brain 0.1 mm below the VD coordinate and retracted back up to the correct level. We infused 1µl of volume at a speed of 0.2 µl/min. After the infusion, the needle was left in place for 3 min before retraction. Animals recovered from the anesthesia in a heated incubator set to 37°C and were monitored until fully recovered. Experimenters were blinded regarding the viral vector genotype.

Behavioral testing

The behavior of animals was assessed with the following tests: narrow beam test, grid test, cylinder test, swing test and tremor assessment. The week prior to surgery, animals received at least 3 pre-training sessions on the narrow beam test. A baseline measurement was obtained 2 days before surgery and the first measurement was performed 1 week after the surgery. During the first 3 weeks post-surgery, all tests were performed twice a week and subsequently once a week until the termination of the experiment. The two investigators scoring the behavior tests were blinded for the treatment groups.

Grid test

The grid test was employed to study forepaw use, in particular the use of distal musculature and digit manipulation which is sensitive to dopaminergic input from the striatum (Tillerson and Miller, 2003). Mice were suspended upside down on a metal grid and allowed to move freely across the grid. A successful trial occurred when the animal held on to the grid for a minimal of 10 seconds and took at least 10 steps. The maximum trial length was 30 seconds. The total number of successful and unsuccessful steps (overshoot, misplacement, loss of grip) with either forepaw was counted by two blinded observers independently. Each animal performed three trials and the average ratio between the total forepaw faults/total forepaw steps over these trials was calculated (Meredith and Kang, 2006).

Cylinder test

The cylinder test was performed to assess preference of front paw use during rearing behavior (Liu et al., 1999; Ulusoy et al., 2009). Animals were allowed to move freely in a glass cylinder for 5 minutes or until they performed 20 full rearing movements. During a successful rearing movement (i.e. the mouse reached at least 5cm from the base of the cylinder), the placement of the right, left or both forepaws was recorded. A new rearing movement was considered only once the mouse had returned its forepaws to the base of the cylinder. Additionally, paw placements were not recorded if the animal's torso was rotated during a rearing movement. The percentage of right paw use was calculated over the total number of the rearing score.

Narrow beam test

The hind limb placement was tested using the narrow beam test adapted from Fleming et al. (2004) and Drucker-Colin and Garcia-Hernandez (1991). Mice crossed an 8 mm wide and 100 cm long beam, elevated 15 cm above a table. The total number of correct hind limb steps and hind limb slips were counted and averaged over 3 complete runs.

Tremor

A semi-subjective tremor assessment was performed during the narrow beam test when animals were stationary on the platforms. A positive tremor score required the

animal to shake while stationary, show a shaky tail when stretched, and unstable and shaky front paw placement when exploring the environment.

Swing test

The swing test was adapted from Roghani et al. (2002) The direction of body rotation was scored by suspending mice 5cm above the bottom of a cage while holding them at the base of their tail for 30 sec. During that time the direction of each swing above a 30° angle was scored.

Tissue processing

Animals were sacrificed by an IP overdose with Pentobarbital (50mg/µl) and transcardially perfused with 0.9% saline followed by 4% paraformaldehyde (PFA, Sigma-Aldrich Co., St. Louis, MO, USA) in sodium phosphate buffer (PBS, Sigma) pH 7.4. The brains were post-fixed overnight, cryoprotected in 30% sucrose/PBS and 6 series of 30µm thick coronal sections containing the SN and striatum were cut on a cryostat. Sections were stored free floating at 4°C in 1% PFA in PBS pH 7.6.

Fluorescent immunohistochemistry

All immunohistochemical (IHC) stainings were performed on free-floating sections. Prior to the staining, sections were blocked in blocking buffer (TBS with 2.5% fetal calf serum (DAKO A/S, Glostrup, Denmark) and 0.2% Triton-X 100 (Sigma)) for 1 hour RT. Sections were incubated with anti-TH antibody (either rabbit polyclonal (1:500; Pel-Freez Biologicals, AR, USA), or mouse monoclonal, clone LNC1 (1:1000; Millipore MAB318, Temecula, CA, USA). The staining was combined with either anti-RGMa (1:100; D-16 sc-46482, Santa Cruz, CA, USA) goat polyclonal antibody, anti-glial fibrillary acidic protein (GFAP)-Cy3 conjugated mouse monoclonal antibody (1:1500;G-A-5, Sigma), anti-Iba1 rabbit polyclonal antibody (1:2000; Wako, Osaka, Japan) or anti-Akt or pAkt antibodies (1:25; 9272 and 4060; Cell Signaling, CA, USA). Primary antibody incubations were performed in blocking buffer for 1 h at RT followed by overnight incubation at 4°C. Alexa 488-, Cy3- and DyLight 680-coupled secondary antibodies (1:800; Invitrogen, Carlsbad, CA, USA) were used for detection of the primary antibodies by incubation for 1h at RT in blocking buffer followed by 20 min incubation in PBS containing Hoechst 33258 (1:10000; BioRad, Hercules, CA, USA). Sections were mounted on gelatin coated glass slides and

embedded in Mowiol (0.1 M Tris pH 8.5, 25% glycerol, 10% w/v Mowiol 4-88 (Sigma)).

TH immunohistochemistry with cresyl violet counterstaining

Sections were blocked as described above, and subsequently incubated with anti-TH rabbit polyclonal antibody (1:500; Pel-Freez Biologicals) blocking buffer for 1 h at RT followed by overnight incubation at 4°C. Next, sections were washed 3 times in TBS and incubated with biotin labeled donkey anti-rabbit antibody (1:400; Vector Laboratories, Burlingame, CA, USA) for 1 hour at RT followed by incubation with ABC Vectastain complex (1:800, Vector Laboratories) in TBS for 1 h. Finally, sections were washed 3 times in TBS and incubated with DAB solution for 10 min, washed in water, mounted onto gelatin coated glass slides and dried overnight at 37°C. Sections were counterstained with 0.1% Cresyl Violet for 30 seconds (Aldrich Chemical Company, Inc. Milwaukee, USA) and subsequently dehydrated through a series of ethanol washes (70%, 80%, 90%, 96%, 2 x 100%; 5 mins each) followed by two xylene washes (10 mins each). Slides were then embedded with Entellan (Merck, Darmstadt, Germany) and allowed to dry overnight before imaging.

Image processing and quantification

Images were acquired with an AxioPlan 2 microscope (Zeiss, Sliedrecht, The Netherlands) with Planapochromat objectives, using Evolution QEi black and white or Evolution MP color camera (MediaCybernetics) and ImagePro software. 10x magnification pictures were taken for SN sections and 2.5x magnification pictures were taken for the striatum sections with fixed exposure times for each channel. The exposure time was selected so the fluorescence signal was not overexposed.

Estimation of neuronal density in the SN

For each animal, 3 sections from one cresyl violet and TH stained series were used for measuring the neuronal density within the SN as described by Bao *et al.* (Bao et al., 2005) and Huitinga et al. (2000). Briefly, the SN pars compacta (SNpc) structure in the non-injected side of the brain was identified at 2.5x magnification using the color camera on the Axioskop microscope. The anatomical borders of the non-injected SN were defined and outlined using the mouse brain atlas (Paxinos, 2001) and the outlined area was projected in a mirror fashion on to the injected SN, with

slight adjustments to fit the anatomy of the contralateral SN. The outlined area was subdivided into a square grid using an Image Pro Plus macro, with each grid field representing one image at 40x magnification. Based on the standard deviation of the number of counted neurons per field, sampling of 35% of the total number of fields was determined sufficient to estimate the neuronal density. Each neuron was identified based on its size and neuronal-like morphology (large and spherical shape) and most importantly the presence of a nucleus with a nucleolus. TH-positive and –negative neurons were counted separately. The total number of neurons counted in the injected and non-injected SN was corrected for the size of the outlined area and thickness of each section to yield the average neuronal number in mm^3. Since neuronal atrophy decreases the size of neuronal cells to be comparable to (small) glial cells, it potentially eliminates atrophied neurons from the counting criteria. This means that a decrease of neuronal density may also reflect neuronal atrophy in additional to neuronal loss.

Fluorescence intensity and area analysis

Mouse SNpc was outlined based on the TH staining and anatomical borders in the ImagePro Plus Measure Threshold macro. Additionally, an area just outside the SNpc was outlined to obtain a measurement of the background fluorescence levels. Total fluorescence intensity of TH, GFAP, and Iba1 was measured in both areas and the background value was subtracted from the fluorescent intensity measured in the SNpc. The total intensity value was then corrected for the size of the outlined area by multiplying the surface area of fluorescence signal, resulting in the average fluorescent intensity value or the integrated optical density. Striatal sections were outlined based on the Hoechst staining and anatomical borders. Here TH, GFAP and Iba1 fluorescence intensity was also measured and corrected for background and size of the area. Finally all sections from one series per each animal (8-10 sections) were averaged, resulting in readout of average fluorescence intensity in the SN or the striatum for each animal.

The total area positive for TH immunofluorescence was outlined and measured using ImagePro Plus in the SNpc and in the background area placed above the SN. Only TH signal higher than 3x the average background fluorescent value of all sections was measured. In case any signal was detected in the background outline, these values were subtracted from the SN area. For each

419 animal an average of TH+ area per section was calculated, with 8 to10 sections
420 measured per animal.
421
422 Akt and pAkt image analysis in TH+ SN neurons
423 Images of sections stained for TH and Akt were analyzed using ImageJ software
424 (National Institutes of Health). The soma of TH positive cells within the SNpc were
425 identified using standardized thresholding. To exclude any axo-dendritic signal, a
426 particle exclusion was applied. The created mask was then superimposed on to the
427 Akt or the pAKT channel, and the average intensity of the Akt or the pAkt signal was
428 determined. An average of 4 sections were quantified per animal.
429
430 **Statistical Analysis**
431 Data analysis was performed in the SPSS software (IBM) or in the GraphPad Prism
432 software. All data are expressed as mean +/- SEM. Statistical analysis was
433 performed using either one way ANOVA with Tukey's multiple testing correction
434 when comparing between more than two animal groups, unpaired student T-test
435 when comparing between the bilaterally injected animal groups, or paired student T-
436 test when comparing SN and striatum within the unilaterally injected animals.
437 Behavioral testing statistical analysis was performed using a two way ANOVA with
438 Tukey's multiple testing correction post hoc analysis. A p value < 0.05 was
439 considered significant for all analyses.
440
441 **Study approval**
442 All animal experimental procedures and postoperative care were carried out in
443 accordance with the Institutional Animal Care and Use Committee of the Royal
444 Netherlands Academy of Arts and Sciences.
445

Results

RGMa and neogenin are expressed by neurons in human post-mortem SN

Gene expression analysis on human post-mortem SN tissue from PD patients and age matched controls showed a 2.1 fold increase in RGMa mRNA expression in the PD SN (Bossers et al., 2009). *In situ* hybridization analysis of the tissue from the same patients used in the gene expression analysis revealed a neuron-specific expression of RGMa mRNA in SN tissue (Figure 1A-C). Immunohistochemical analysis, using an antibody recognizing the C-terminal fragment of RGMa, revealed a punctate expression of RGMa protein in tyrosine hydroxylase positive (TH+) neurons and in the surrounding extracellular space, suggesting release of RGMa (Figure 1D-E). Cellular expression and release of RGMa in the extracellular environment, including the C terminal and N-terminal fragments, has also been shown in multiple sclerosis patients (Demicheva et al., 2015). Human SN neurons also express the RGMa receptor neogenin (Figure 1F-G).

AAV-mediated delivery of RGMa results in enhanced RGMa levels in the SN and transport of RGMa to the striatum

Based on the specific neuronal expression of RGMa in human SN, we constructed an AAV vector driving mouse RGMa expression specifically in neurons using a synapsin promotor. AAV-synapsin-driven expression of mouse RGMa protein was validated after transfecting N2A cells with this construct. We detected the full length membrane bound form (55 – 49kDa) and the cleaved membrane bound C-terminal form (33kDa) of RGMa in the cell lysate, as well as the 30kDa N-terminal fragment of RGMa in the culture medium of the N2A cells (Figure 2A). This pattern of expression and release is consistent with the report of Tassew et al. (2012).

Increased RGMa protein levels were observed both after high and low titer stereotactic injection of the AAV-RGMa vector in the SN. As expected, the injection of high titer virus resulted in two times higher RGMa protein levels compared to the low titer viral injection (Figure 2B, $p<0.0001$, $F(3,22) = 41.21$). High titer AAV-RGMa injection resulted in an increase in the protein levels in both the SN and the striatum of the bilateral and unilateral AAV-RGMa injected animals (Figure 3A). Similarly, in the low titer treatment paradigm, increased RGMa protein levels were observed both

in the SN and the striatum of the AAV-RGMa injected animals (Figure 3B), but not in the AAV-Empty, AAV-GFP or saline injected animals. RGMa was expressed in DA-neurons as well as extracellularly, confirming the release of the protein. Example images used for the quantification of RGMa are shown in Figure 6B (high dose experiment) and 7B (low dose experiment). These results are indicative of successful AAV-mediated overexpression of RGMa in the SN.

RGMa overexpression in the SN induces severe motor impairments

We next investigated whether overexpression of RGMa in the SN affects motor performance in mice. Animals injected with a high dose of AAV-RGMa (at a titer of $9.0x10^{12}$ gc/ml) either uni- or bilaterally in the SN developed severe motor deficits over time (Figure 4A-D). No motor deficits were observed in the control animals, bilaterally injected with titer matched AAV-Empty virus. The most striking behavioral deficit was revealed by the grid test, which is designed to measure accuracy of front paw placement and is significantly correlated with striatal dopamine levels (Tillerson and Miller, 2003). Both unilaterally and bilaterally AAV-RGMa injected animals performed progressively worse in this test ($p<0.0001$, $F(2,270) = 49.97$) compared to the AAV-Empty control group. By 2.5 weeks post-injection motor deficits started to be evident in the animals overexpressing RGMa and they progressively worsened until the end of the experiment at week 18.5 (Figure 4A). The narrow beam test (Drucker-Colin and Garcia-Hernandez, 1991; Fleming et al., 2004) showed a significant increase in the number of hind limb errors made by the unilaterally AAV-RGMa injected animals ($p<0.0001$, $F(2,270) = 46.52$), already starting 2 weeks post-surgery (Figure 4B).

In the cylinder test (Liu et al., 1999; Ulusoy et al., 2009), mice overexpressing RGMa either uni- or bilaterally developed a significant preference of single right paw use during rearing behavior ($p<0.0001$, $F(2,240) = 46.96$, Figure 4C). Additionally, the bilaterally treated RGMa group also showed a significant increase ($p<0.0001$, $F(2,240) = 18.84$) in the use of their left paw over the use of both paws suggestive of a dysfunction in coordinated use of both forepaws in this group (data not shown). This was not the case for the unilaterally injected animals; as expected, single left paw use was not increased compared to use of both paws together indicative of the contralateral effects of injection of AAV-RGMa in the right SN. Animals injected with AAV-Empty did not develop a preference in single paw use. The swing test (Roghani

et al., 2002) revealed a significant preference in turning towards the left (contralateral to the side of the lesion) in unilaterally AAV-RGMa injected animals ($p<0.0001$, $F(2,195) = 57.19$, Figure 4D). As expected, the bilateral RGMa group did not develop a side preference in the swing test given that both SN were targeted. Similarly, AAV-Empty injected animals did not develop a side preference in the swing test.

In conclusion, all motor behavioral tests revealed motor impairments in mice overexpressing RGMa in the SN, but to a different degree depending on whether RGMa was delivered unilaterally or bilaterally. Additionally, a tremor assessment indicated significantly more tremor events in AAV-RGMa-injected animals ($p<0.0001$, $F(2,240) = 55.58$, Figure 4E). Bilateral RGMa overexpression had a negative impact on body weight, but this was only evident from 12.5 weeks on during the experiment ($p<0.0001$, $F(2,360) = 42.86$, Figure 4F), and can thus not be responsible for the behavioral changes that are observed at earlier time points.

Low dose RGMa overexpression induces subtle behavioral deficits

We show above that overexpression of RGMa in the SN induces severe motor deficits. To test the potency of the RGMa effect, we hypothesized that administration of a lower dose of RGMa would result in the development of more subtle motor deficits in mice and therefore mimic more closely the gradual progressive nature of the clinical symptoms in PD. To this end mice were injected with a viral vector titer of $3.0x10^{12}$ gc/ml, which is three times lower than the high dose RGMa overexpressing experiment described above. Animals injected with this lower titer of AAV-RGMa virus in the right SN developed more subtle progressive behavioral motor deficits as measured in the grid and cylinder tests (Figure 5). No motor deficits were observed in the control groups injected with either saline, or titer matched AAV-Empty or AAV-GFP viruses. The most striking behavioral deficit was revealed by the grid test in which RGMa overexpressing animals performed progressively worse ($p<0.0001$, $F(3,400) = 61.31$, Figure 5A), compared to the three control groups. The dysfunction started at 3.5 weeks and remained present until the end of the experiment at week 12 (Figure 5A). At week 12, RGMa animals showed some degree of recovery, but still performed significantly worse than the AAV-GFP injected animals.

In the cylinder test, during the course of the experiment, mice overexpressing RGMa developed a significant preference for single right paw use during rearing compared to the control injected animals ($p<0.0001$, $F(3,375) = 12.37$, Figure 5C).

This suggests a dysfunction of the left front paw, caused by low dose RGMa overexpression in the contralateral SN.

The narrow beam test revealed small but significant impairment in hind limb placement after low dose RGMa expression ($p=0.0002$, $F(3,416) = 6.586$, Figure 5B). In contrast to the high dose RGMa experiment, the swing test did not reveal a preference in turning behavior in any of the treatment groups in the low dose experiment (Figure 5D). A tremor assessment indicated more positive events in the AAV-RGMa injected animals starting 3.5 weeks post-surgery ($p<0.0001$, $F(3,416) = 20.71$, Figure 5E). Finally, unilateral low dose RGMa overexpression had no impact on body weight (Figure 5F). In summary, the extent of motor impairment in mice injected with the low titer AAV-RGMa virus is less dramatic than in mice injected with a high titer AAV-RGMa virus.

RGMa decreases neuronal density in the SN

We next investigated the effects of RGMa overexpression on SN neuronal integrity. Neuronal density was determined in cresyl violet and TH stained sections. High levels of bilateral RGMa overexpression in the SN resulted in 24% reduction in the total neuronal densities (TH positive (TH+) and other neurons combined, $p=0.0136$) and in 38% reduction of TH+ neuronal densities ($p=0.012$), compared to the AAV-Empty bilaterally injected control mice (Figure 6A). Unilateral high titer AAV-RGMa injection into the right SN resulted in a significant decrease of 18% in the total neuronal density ($p=0.004$), and a 40% decrease of TH+ neuronal density compared to the left non injected SN ($p=0.0072$, Figure 6A). Importantly, TH negative (TH-) neuron numbers were not affected by RGMa overexpression in either of the experimental groups ($p=0.67$, $p=0.53$).

Similarly, in the low titer RGMa overexpressing experiment, a 22% decrease in the total neuron numbers ($p=0.0029$) and a 30% decrease in the TH+ neuron numbers ($p=0.0018$) was revealed in the injected SN in animals overexpressing RGMa compared to the contralateral non-injected SN at 12 weeks post injection (Figure 7A). In animals injected with AAV-Empty or AAV-GFP no changes in neuronal density were observed (Figure 7A). Overexpression of RGMa in the SN compared to the AAV-Empty and AAV-GFP injected SN resulted in a significant decrease in the total neuronal densities (23 and 26% respectively, $p=0.0015$, $F(2, 19) = 9.318$) and in the total density of TH+ neurons (30 and 33% respectively,

p=0.0041, F (2, 19) = 7.449) (Figure 7A). As seen in the high dose experiments, RGMa overexpression did not affect the density of the TH- neurons within the SN to a large extent, except when compared to AAV-GFP injected SN, showing a small, yet significant decrease in the density of TH- neurons after RGMa overexpression (p=0.0488, F (2, 19) = 3.555, Figure 7A).

RGMa induced degeneration of TH-positive neurons and upregulation of TH in surviving DA-neurons

RGMa overexpression in the mouse SN was accompanied by a significant decrease in TH+ area within the SN as compared with the AAV-Empty injected SN (p=0.0005, Figure 6B and C) and as compared with the non-injected SN in the unilateral treatment group (p=0.0026, Figure 6B and C). We also quantified the TH fluorescence intensity levels over the entire SN. To our surprise, the TH fluorescence levels in the AAV-RGMa injected SN of the bilateral treated animals were not significantly decreased compared to the AAV-Empty control animals (Figure 6D). This, in conjunction with the decrease in TH+ neurons observed in these treatment conditions (Figure 6A) is suggestive of a compensatory increase in TH expression in the surviving DA neurons of the injected SN. Moreover, the TH fluorescence levels in the non-injected SN of the unilateral AAV-RGMa treated animals were significantly increased compared to the injected right SN (p=0.006) This is, again, suggestive of a compensatory effect, this time in the DA neurons of the contralateral (non-injected) SN, as a result of TH depletion in the injected SN in unilateral AAV-RGMa treated animals.

Striatal TH fluorescence levels showed a significant decrease in the right striatum of the animals overexpressing RGMa unilaterally when compared to the left striatum (p=0.0004, Figure 6E and F), and in both striata in the animals overexpressing RGMa bilaterally when compared to the AAV-Empty animals (p=0.0085, Figure 6E and F). The decrease in striatal TH levels in RGMa-injected SN (unilaterally or bilaterally) supports the observed behavioral deficits in these animals. Although the TH levels of the contralateral SN in unilaterally AAV-RGMa injected animals were increased compared to TH levels in the injected SN, this did not translate to a similar increase in striatal TH levels. The presumed compensatory effect occurring in the contralateral, therefore non-injected SN of unilaterally treated animals seems to be limited to the SN.

Comparable to the high dose, low dose RGMa overexpression also resulted in a significant decrease of the TH+ area in the injected SN compared to the non-injected SN ($p=0.0048$) and to the AAV-Empty, AAV-GFP and saline injected SN ($p=0.0012$, $F(3, 21) = 7.692$, Figure 7B and C). The non-injected SN of the RGMa treated mice showed a trend towards a decrease in TH+ area compared to the control treatment non-injected SN, which is most likely caused by a minor spread of the viral vector to the contralateral SN (Figure 7B). Similar to the high dose experiment, we did not see a decrease in the intensity of the TH signal in AAV-RGMa injected animals. In contrast, the TH fluorescence levels in the contralateral (non-injected) SN of animals treated with AAV-RGMa were strongly increased when compared to all of the control groups ($p=0.0006$, $F(3, 23) = 8.3$) and when compared to the injected SN ($p= 0.038$, Figure 7D). In contrast to the high dose experiment, this increase was also observed in the striatum: TH fluorescence levels of nigrostriatal axons and terminals in the left striatum (the projection area of the left, non-injected SN neurons) were significantly increased in AAV-RGMa treated animals compared to the right striatum ($p=0.0037$) or to the left striatum of the AAV-GFP treated animals ($p=0.0082$, Figure 7E and F). The right striatum, the projection area of the right, injected SN, did not show a significant decrease in TH fluorescence levels as a result of RGMa overexpression when compared to the GFP-transduced nigrostriatal terminals ($p=0.6139$). These observations suggest that surviving DA neurons in the injected SN are increasing their TH production as a possible compensatory mechanism to overcome the progressive decrease in DA levels within the nigrostriatal system. This may explain why the behavioral deficits in the low dose paradigm (Figure 5) are not as severe as in the high dose paradigm (Figure 4). Additionally, it is important to note that, in the low dose experiment, TH levels were measured in the striatum at the end of the experiment (at week 12) when some behavioral deficits show signs of recovery (Figure 5A). Animals treated with a high dose of AAV-RGMa do not display a recovery in motor function (Figure 4), consistent with the decreased levels of TH fluorescence measured in the striatum of these animals at the end of the high dose experiment (week 18.5; Figure 6E and F). Perhaps analysis of the TH levels in the striatum at an earlier stage after low dose RGMa administration, e.g. between week 7 to 9, would have resulted in a detectible decrease in TH levels consistent with this worsened level of behavioral ability observed at those time points.

RGMa overexpression induces gliosis

To investigate whether RGMa overexpression has an effect on the glial response in the SN, we analyzed the expression of the astrocytic marker GFAP and the active microglial marker Iba1 at 18.5 weeks post-injection in the high dose paradigm (Figure 8A-C). Both GFAP and Iba1 fluorescence levels were increased in SN injected either unilaterally (GFAP p=0.0004, Iba1 p= 0.04, Figure 8B) or bilaterally (GFAP p=0.005, Iba1 p=0.001, Figure 8C) with AAV-RGMa when compared to the non-injected SN or to the injected SN of the AAV-Empty animals respectively.

Overall, no substantial microgliosis was observed in the striatum of mice overexpressing RGMa in the SN, although there was a small but significant decrease in GFAP signal in the right striatum of animals in the unilateral injection paradigm (p=0.027, Figure 8D), and a small significant decrease of Iba1 signal in the striatum of animals overexpressing RGMa bilaterally (p=0.015, Figure 8E).

Furthermore, to investigate whether low dose RGMa overexpression has an effect on the glial response, we analyzed the expression of GFAP and Iba1 in these animals 12 weeks post-injection (Figure 9A-C). Similarly to the high titer experiment, GFAP fluorescence levels were increased in SN injected with AAV-RGMa compared to both the non-injected SN ($p<0.0001$) and to the injected SN of the AAV-GFP animals ($p=0.0020$, $F(3, 25) = 6.583$, Figure 9A and B). Additionally we found an induced activation of microglia in AAV-RGMa injected SN compared to the non-injected SN ($p<0.0001$, 9A and C) as well as compared to AAV-Empty and saline control treatment groups ($p<0.0001$, $F(3, 25) = 19.66$). No microgliosis was seen in the striatum of mice injected in the SN with AAV-RGMa (data not shown).

In addition to RGMa-associated SN gliosis, an increase in microglial activation was seen in AAV-GFP injected animals in both injected ($p<0.0001$, $F(3, 25) = 19.66$) and non-injected SN 12 weeks post-injection ($p<0.0001$, $F(3, 25) = 35.26$, Figure 9A-C) suggesting an immune response to the GFP protein, as previously reported by others (Klein et al., 2006; Yang et al., 2016). AAV-GFP injected animals also showed a significant decrease in GFAP fluorescence intensity in the non-injected SN compared to the other control treatment groups ($p<0.0001$, $F(3, 25) = 32.97$, Figure 9A, B).

RGMa expression in the SN does not decrease phosphoAKT in DA neurons

Akt is an anti-apoptotic factor which has been shown to be dephosporylated in neurons that are degenerating following exposure to RGMa-derived from Th17 cells in culture (Tanabe and Yamashita, 2014). To determine whether RGMa induces DA-neuron degeneration via pAKT we examined the phosphorylation state of Akt using pAKT specific antibodies in the DA neurons following overexpression of RGMa. The levels of total AKT protein and pAKT were not different in DA neurons identified by TH immunohistochemistry (Figure 10). These data suggest that phosphorylation of AKT is not affected by RGMa and that this cell death pathway is not involved in RGMa-induced DA neuron degeneration.

Discussion

The upregulation of RGMa in the SN of PD patients and its role in axon repulsion and neuronal survival prompted us to study the consequences of increased RGMa levels in the mesencephalic dopaminergic system of mice. We show that AAV-mediated overexpression of RGMa by midbrain dopaminergic neurons induced degeneration of these neurons resulting in a movement disorder typical for striatal DA deficiency. RGMa overexpression also induced strong astro- and microglial activation. These data implicate RGMa in the pathophysiology of PD and suggest that targeting RGMa signaling could have therapeutic potential for the treatment of PD.

RGMa induced degeneration of mouse SN – similarities to PD etiology

The effects of overexpression of RGMa in the mouse midbrain bear several striking commonalities with the neuropathology of PD. Upregulation of RGMa in the adult mouse SN, both at high and low levels, induced progressive movement deficits, albeit at different severity, due to DA loss in the striatum (Tillerson and Miller, 2003) mimicking the clinical motor symptoms of PD patients. Additionally, we observed a preferential loss of TH+ neurons in the targeted SN, whereas TH- neurons were unaffected. This TH+ neuronal loss was observed in both high and low dose RGMa overexpressing animals. Selective degeneration of TH+ neurons and the sparing of TH- neuronal populations including calbindin positive neurons in the SN is a hallmark of the disease (Yamada et al., 1990; Kordower et al., 2013) and has also been observed in other animal models for PD, such as MPTP-treated monkeys (Lavoie and Parent, 1991; German et al., 1992). Interestingly, in unilateral high dose RGMa expressing animals, the striatal TH levels on the injected side were decreased compared to the contralateral side, whereas TH levels in the non-injected SN were increased compared to the injected side. This may suggest that the unaffected SN is compensating for loss of DA signaling in the contralateral nigrostriatal pathway by upregulating TH protein levels as a means to increase DA production. Furthermore, in low dose RGMa overexpressing mice, in which slightly less severe DA neuron loss is observed, TH protein levels were also increased in the non-injected SN and the non-affected striatum, suggestive of the development of a compensatory mechanism in spared DA neurons. Such a compensatory mechanism, aimed to combat the

diminishing DA levels in the nigrostriatal pathway, may explain the observed trend towards a less severe behavioral phenotype and some degree of functional recovery as observed in these low dose RGMa animals in the grid test 12 weeks post-surgery. A similar mechanism has been previously described in low dose MPTP-treated asymptomatic primates where surviving dopaminergic neurons enhanced their dopamine release into the striatum (Perez et al., 2008). Moreover, in a “low dose” synucleinopathy model for PD, striatal TH expression returned to baseline levels following an initial decrease, correlating with a rescue of behavioral deficits (Koprich et al., 2011).

To further investigate the commonalities between RGMa-induced cellular changes in the mouse nigrostriatal system and neuropathology in PD we studied an other pathological feature that is prominent in PD - glial reactivity (Langston et al., 1999; Hanisch, 2002; Barcia et al., 2003; Hirsch et al., 2003; McGeer and McGeer, 2008; Mosley et al., 2012). RGMa induced both astro- and microgliosis in the mouse SN. In PD, gliosis may play a crucial role in the progression of neuronal degeneration by increasing the release of cytokines and chemokines from activated glia cells (Hanisch, 2002; Barcia et al., 2003; Hirsch et al., 2003; Mosley et al., 2012). Indeed, treatments that prevent microglia activation in the MPTP mouse model (Schintu et al., 2009), or reduce pro-inflammatory cytokine release in the 6-OHDA rat model (Smith et al., 2015) have been shown to promote dopaminergic neuron survival *in vivo*.

Possible mechanisms of RGMa induced neurodegeneration

Based on the known functions of RGMa, we discuss two scenarios how the current neurodegenerative phenotype might develop. Following neuron-specific overexpression of RGMa in the SN, we observed elevated RGMa protein levels in the SN and in the ipsilateral striatum indicative of RGMa protein transport via nigrostriatal projections. The increased levels of RGMa may have significant implications for RGMa-neogenin signaling within the nigrostriatal system.

In the first scenario, the increased levels of RGMa protein in the striatum may induce repulsive signaling in the dopaminergic nigrostriatal projections leading to synaptic loss, axonal retraction, and finally atrophy and/or neuronal death in the SN. RGMa-induced axonal repulsion occurs when RGMa signals through neogenin to induce growth cone collapse (Wilson and Key, 2007; Yamashita et al., 2007).

RhoA/Rho-kinase and PKC become activated, and downstream myosin II phosphorylation leads to a reduction of F-actin in growth cones and subsequent axonal collapse (Conrad et al., 2007; Kubo et al., 2008). Furthermore, RGMa acting through neogenin can also inhibit outgrowth and repulsion of neurites of cortical neurons by inducing growth cone collapse (Endo and Yamashita, 2009). The induction of retrograde neuronal death and/or atrophy would be in support of the dying back hypothesis (Dauer and Przedborski, 2003; Cheng et al., 2010; Maday, 2016; Tagliaferro and Burke, 2016), stating that the primary neurodegenerative event in PD is the loss of dopaminergic nigrostriatal presynaptic terminals followed by the subsequent retraction of axons, degeneration of dopaminergic neurons in the SN and induction of a glial response.

In the second scenario, increased RGMa expression in neurons would lead to local RGMa signaling in the SN where it could interact with neogenin expressed on DA neurons and/or attract and activate immune cells which express neogenin. In the human brain RGMa is associated with DA neurons and is present in extracellular deposits, whereas after forced overexpression in the mouse RGMa is expressed in DA neurons and in a diffuse extracellular pattern. This suggest that RGMa can act as a short range as well as a long range cue in the SN. RGMa-neogenin signaling in immune cells can lead to the production of pro-inflammatory cytokines which consequently can induce neuronal toxicity. The role of the immune system in terms of a pathological feature of PD has gained much attention in recent years (reviewed in Kannarkat et al., 2013). There is evidence of increased CD4+ and CD8+ T cell numbers in the SN of PD patients (Brochard et al., 2009), and an increase in CD4+ T cell infiltration into the SN in the MPTP model has also been observed (Reynolds et al., 2010). Neogenin is expressed by various non-neuronal cells, including $CD4^+$ T cells and macrophages in a mouse MS model (Muramatsu et al., 2011) and by $CD3^+$ T cells in the brain and the spinal cord of MS patients (Muramatsu et al., 2011). Furthermore, T cell recruitment to active lesion areas in the MS mouse model has been shown to be mediated through RGMa binding to its receptor neogenin (Muramatsu et al., 2011; Tanabe and Yamashita, 2014). Therefore, RGMa released by dopaminergic neurons may result in the activation of immune cells and induce cytokine and chemokine production, which leads to neuronal stress and neurotoxicity. Consequently, RGMa overexpression-mediated recruitment of these pro-inflammatory cells could induce neuronal degeneration in the mouse SN.

In summary, we identified RGMa as a new key player in dopaminergic neuron degeneration in the adult SN. The data suggest that RGMa may have a crucial role in the development of PD pathology. A recent pilot study reports that levodopa increased RGMa levels in blood plasma of PD patients, which may further inhibit mechanisms of neuronal survival (31). Various axon guidance cues, with important roles during neuronal development, are now being linked to the pathophysiology of neurodegenerative diseases including semaphorins, ephrins, slits and netrins and their respective receptors (reviewed in Korecka et al., 2015; Van Battum et al., 2015). Changes in the expression levels or expression patterns of these axon guidance cues might induce alterations in the neuronal circuitry thereby contributing to the development of the neuropathology. The current findings have implications for therapy development as interfering with the function of this specific guidance cue may be beneficial to the survival of DA neurons. Given the fact that the use of anti-RGMa antibodies in disease models such as MS (Tanabe and Yamashita, 2014; Demicheva et al., 2015) or stroke (Shabanzadeh et al., 2015) has led to functional improvements, our findings point to RGMa as a promising therapeutic target for PD and RGMa monoclonal antibodies may be applied as a disease modifying treatment for PD.

Author contributions

JK- experimental design, experimental execution, acquiring data, analyzing data, writing the manuscript
EM- experimental execution, acquiring data, analyzing data, writing the manuscript
RE- experimental execution, experimental design
BH-experimental execution
SS- experimental execution, acquiring data, analyzing data
NRV- experimental execution, acquiring data, analyzing data
RP- experimental design, providing reagents
DS- experimental design,
AS- experimental design,
RK- experimental design,
KB- experimental design, experimental execution, help with analyzing the data, writing the manuscript
JV- experimental design, writing the manuscript

Acknowledgments

We acknowledge the financial support of the Stichting ParkinsonFonds, Top Institute Pharma and Stichting Vrienden van het Herseninstituut. We would also like to thank Prof. Deniz Kirik (Lund University, Sweden) for providing us with pAAV2Sna-SW and pTRUF20B-SEW plasmids.

References

Bao AM, Hestiantoro A, Van Someren EJ, Swaab DF, Zhou JN (2005) Colocalization of corticotropin-releasing hormone and oestrogen receptor-alpha in the paraventricular nucleus of the hypothalamus in mood disorders. Brain : a journal of neurology 128:1301-1313.

Barcia C, Fernandez Barreiro A, Poza M, Herrero MT (2003) Parkinson's disease and inflammatory changes. Neurotoxicity research 5:411-418.

Biosciences N (2012) Human body index- transplictional profiling. In.

Bossers K, Meerhoff G, Balesar R, van Dongen JW, Kruse CG, Swaab DF, Verhaagen J (2009) Analysis of gene expression in Parkinson's disease: possible involvement of neurotrophic support and axon guidance in dopaminergic cell death. Brain pathology 19:91-107.

Braak H, Del Tredici K, Rub U, de Vos RA, Jansen Steur EN, Braak E (2003) Staging of brain pathology related to sporadic Parkinson's disease. Neurobiology of aging 24:197-211.

Brochard V, Combadiere B, Prigent A, Laouar Y, Perrin A, Beray-Berthat V, Bonduelle O, Alvarez-Fischer D, Callebert J, Launay JM, Duyckaerts C, Flavell RA, Hirsch EC, Hunot S (2009) Infiltration of CD4+ lymphocytes into the brain contributes to neurodegeneration in a mouse model of Parkinson disease. The Journal of clinical investigation 119:182-192.

Capelli LP, Krepischi AC, Gurgel-Giannetti J, Mendes MF, Rodrigues T, Varela MC, Koiffmann CP, Rosenberg C (2012) Deletion of the RMGA and CHD2 genes in a child with epilepsy and mental deficiency. European journal of medical genetics 55:132-134.

Cheng HC, Ulane CM, Burke RE (2010) Clinical progression in Parkinson disease and the neurobiology of axons. Annals of neurology 67:715-725.

Cole SJ, Bradford D, Cooper HM (2007) Neogenin: A multi-functional receptor regulating diverse developmental processes. The international journal of biochemistry & cell biology 39:1569-1575.

Conrad S, Genth H, Hofmann F, Just I, Skutella T (2007) Neogenin-RGMa signaling at the growth cone is bone morphogenetic protein-independent and involves RhoA, ROCK, and PKC. The Journal of biological chemistry 282:16423-16433.

Cooper-Knock J, Kirby J, Ferraiuolo L, Heath PR, Rattray M, Shaw PJ (2012) Gene expression profiling in human neurodegenerative disease. Nature reviews Neurology 8:518-530.

Dauer W, Przedborski S (2003) Parkinson's disease: mechanisms and models. Neuron 39:889-909.

Demicheva E et al. (2015) Targeting repulsive guidance molecule A to promote regeneration and neuroprotection in multiple sclerosis. Cell reports 10:1887-1898.

Drucker-Colin R, Garcia-Hernandez F (1991) A new motor test sensitive to aging and dopaminergic function. Journal of neuroscience methods 39:153-161.

Edwards YJ, Beecham GW, Scott WK, Khuri S, Bademci G, Tekin D, Martin ER, Jiang Z, Mash DC, ffrench-Mullen J, Pericak-Vance MA, Tsinoremas N, Vance JM (2011) Identifying consensus disease pathways in Parkinson's disease using an integrative systems biology approach. PloS one 6:e16917.

Endo M, Yamashita T (2009) Inactivation of Ras by p120GAP via focal adhesion kinase dephosphorylation mediates RGMa-induced growth cone collapse. The Journal of neuroscience : the official journal of the Society for Neuroscience 29:6649-6662.

887 Fleming SM, Salcedo J, Fernagut PO, Rockenstein E, Masliah E, Levine MS, Chesselet MF
888 (2004) Early and progressive sensorimotor anomalies in mice overexpressing wild-
889 type human alpha-synuclein. The Journal of neuroscience : the official journal of the
890 Society for Neuroscience 24:9434-9440.
891 Gao GP, Alvira MR, Wang L, Calcedo R, Johnston J, Wilson JM (2002) Novel adeno-
892 associated viruses from rhesus monkeys as vectors for human gene therapy.
893 Proceedings of the National Academy of Sciences of the United States of America
894 99:11854-11859.
895 German DC, Manaye KF, Sonsalla PK, Brooks BA (1992) Midbrain dopaminergic cell loss
896 in Parkinson's disease and MPTP-induced parkinsonism: sparing of calbindin-D28k-
897 containing cells. Annals of the New York Academy of Sciences 648:42-62.
898 Gorell JM, Peterson EL, Rybicki BA, Johnson CC (2004) Multiple risk factors for
899 Parkinson's disease. Journal of the neurological sciences 217:169-174.
900 Hanisch UK (2002) Microglia as a source and target of cytokines. Glia 40:140-155.
901 Hata K, Fujitani M, Yasuda Y, Doya H, Saito T, Yamagishi S, Mueller BK, Yamashita T
902 (2006) RGMa inhibition promotes axonal growth and recovery after spinal cord
903 injury. The Journal of cell biology 173:47-58.
904 Hermens WT, ter Brake O, Dijkhuizen PA, Sonnemans MA, Grimm D, Kleinschmidt JA,
905 Verhaagen J (1999) Purification of recombinant adeno-associated virus by iodixanol
906 gradient ultracentrifugation allows rapid and reproducible preparation of vector stocks
907 for gene transfer in the nervous system. Human gene therapy 10:1885-1891.
908 Hernandez DG, Reed X, Singleton AB (2016) Genetics in Parkinson disease: Mendelian
909 versus non-Mendelian inheritance. Journal of neurochemistry.
910 Hirsch EC, Breidert T, Rousselet E, Hunot S, Hartmann A, Michel PP (2003) The role of
911 glial reaction and inflammation in Parkinson's disease. Annals of the New York
912 Academy of Sciences 991:214-228.
913 Huitinga I, van der Cammen M, Salm L, Erkut Z, van Dam A, Tilders F, Swaab D (2000) IL-
914 1beta immunoreactive neurons in the human hypothalamus: reduced numbers in
915 multiple sclerosis. Journal of neuroimmunology 107:8-20.
916 Jankovic J (2008) Parkinson's disease: clinical features and diagnosis. Journal of neurology,
917 neurosurgery, and psychiatry 79:368-376.
918 Kalia LV, Lang AE (2015) Parkinson's disease. Lancet 386:896-912.
919 Kannarkat GT, Boss JM, Tansey MG (2013) The role of innate and adaptive immunity in
920 Parkinson's disease. Journal of Parkinson's disease 3:493-514.
921 Klein RL, Dayton RD, Leidenheimer NJ, Jansen K, Golde TE, Zweig RM (2006) Efficient
922 neuronal gene transfer with AAV8 leads to neurotoxic levels of tau or green
923 fluorescent proteins. Molecular therapy : the journal of the American Society of Gene
924 Therapy 13:517-527.
925 Koeberle PD, Tura A, Tassew NG, Schlichter LC, Monnier PP (2010) The repulsive
926 guidance molecule, RGMa, promotes retinal ganglion cell survival in vitro and in
927 vivo. Neuroscience 169:495-504.
928 Koprich JB, Johnston TH, Huot P, Reyes MG, Espinosa M, Brotchie JM (2011) Progressive
929 neurodegeneration or endogenous compensation in an animal model of Parkinson's
930 disease produced by decreasing doses of alpha-synuclein. PloS one 6:e17698.
931 Kordower JH, Olanow CW, Dodiya HB, Chu Y, Beach TG, Adler CH, Halliday GM, Bartus
932 RT (2013) Disease duration and the integrity of the nigrostriatal system in Parkinson's
933 disease. Brain : a journal of neurology 136:2419-2431.
934 Korecka JA, Levy S, Isacson O (2015) In vivo modeling of neuronal function, axonal
935 impairment and connectivity in neurodegenerative and neuropsychiatric disorders
936 using induced pluripotent stem cells. Molecular and cellular neurosciences.

937 Kubo T, Tokita S, Yamashita T (2012) Repulsive guidance molecule-a and demyelination:
938 implications for multiple sclerosis. Journal of neuroimmune pharmacology : the
939 official journal of the Society on NeuroImmune Pharmacology 7:524-528.
940 Kubo T, Endo M, Hata K, Taniguchi J, Kitajo K, Tomura S, Yamaguchi A, Mueller BK,
941 Yamashita T (2008) Myosin IIA is required for neurite outgrowth inhibition produced
942 by repulsive guidance molecule. Journal of neurochemistry 105:113-126.
943 Kumaran R, Cookson MR (2015) Pathways to Parkinsonism Redux: convergent
944 pathobiological mechanisms in genetics of Parkinson's disease. Human molecular
945 genetics 24:R32-44.
946 Lah GJ, Key B (2012) Dual roles of the chemorepellent axon guidance molecule RGMa in
947 establishing pioneering axon tracts and neural fate decisions in embryonic vertebrate
948 forebrain. Developmental neurobiology 72:1458-1470.
949 Langston JW, Forno LS, Tetrud J, Reeves AG, Kaplan JA, Karluk D (1999) Evidence of
950 active nerve cell degeneration in the substantia nigra of humans years after 1-methyl-
951 4-phenyl-1,2,3,6-tetrahydropyridine exposure. Annals of neurology 46:598-605.
952 Lavoie B, Parent A (1991) Dopaminergic neurons expressing calbindin in normal and
953 parkinsonian monkeys. Neuroreport 2:601-604.
954 Lesnick TG, Papapetropoulos S, Mash DC, Ffrench-Mullen J, Shehadeh L, de Andrade M,
955 Henley JR, Rocca WA, Ahlskog JE, Maraganore DM (2007) A genomic pathway
956 approach to a complex disease: axon guidance and Parkinson disease. PLoS genetics
957 3:e98.
958 Lin L, Lesnick TG, Maraganore DM, Isacson O (2009) Axon guidance and synaptic
959 maintenance: preclinical markers for neurodegenerative disease and therapeutics.
960 Trends in neurosciences 32:142-149.
961 Liu Y, Kim D, Himes BT, Chow SY, Schallert T, Murray M, Tessler A, Fischer I (1999)
962 Transplants of fibroblasts genetically modified to express BDNF promote
963 regeneration of adult rat rubrospinal axons and recovery of forelimb function. The
964 Journal of neuroscience : the official journal of the Society for Neuroscience 19:4370-
965 4387.
966 Maday S (2016) Mechanisms of neuronal homeostasis: Autophagy in the axon. Brain
967 research.
968 Matsunaga E, Chedotal A (2004) Repulsive guidance molecule/neogenin: a novel ligand-
969 receptor system playing multiple roles in neural development. Development, growth
970 & differentiation 46:481-486.
971 Matsunaga E, Nakamura H, Chedotal A (2006) Repulsive guidance molecule plays multiple
972 roles in neuronal differentiation and axon guidance. The Journal of neuroscience : the
973 official journal of the Society for Neuroscience 26:6082-6088.
974 Matsunaga E, Tauszig-Delamasure S, Monnier PP, Mueller BK, Strittmatter SM, Mehlen P,
975 Chedotal A (2004) RGM and its receptor neogenin regulate neuronal survival. Nature
976 cell biology 6:749-755.
977 McGeer PL, McGeer EG (2008) Glial reactions in Parkinson's disease. Movement disorders :
978 official journal of the Movement Disorder Society 23:474-483.
979 Meredith GE, Kang UJ (2006) Behavioral models of Parkinson's disease in rodents: a new
980 look at an old problem. Movement disorders : official journal of the Movement
981 Disorder Society 21:1595-1606.
982 Metzger M, Conrad S, Skutella T, Just L (2007) RGMa inhibits neurite outgrowth of
983 neuronal progenitors from murine enteric nervous system via the neogenin receptor in
984 vitro. Journal of neurochemistry 103:2665-2678.
985 Minones-Moyano E, Porta S, Escaramis G, Rabionet R, Iraola S, Kagerbauer B, Espinosa-
986 Parrilla Y, Ferrer I, Estivill X, Marti E (2011) MicroRNA profiling of Parkinson's

disease brains identifies early downregulation of miR-34b/c which modulate mitochondrial function. Human molecular genetics 20:3067-3078.

Monnier PP, Sierra A, Macchi P, Deitinghoff L, Andersen JS, Mann M, Flad M, Hornberger MR, Stahl B, Bonhoeffer F, Mueller BK (2002) RGM is a repulsive guidance molecule for retinal axons. Nature 419:392-395.

Mosley RL, Hutter-Saunders JA, Stone DK, Gendelman HE (2012) Inflammation and adaptive immunity in Parkinson's disease. Cold Spring Harbor perspectives in medicine 2:a009381.

Mueller BK, Yamashita T, Schaffar G, Mueller R (2006) The role of repulsive guidance molecules in the embryonic and adult vertebrate central nervous system. Philosophical transactions of the Royal Society of London Series B, Biological sciences 361:1513-1529.

Muramatsu R, Kubo T, Mori M, Nakamura Y, Fujita Y, Akutsu T, Okuno T, Taniguchi J, Kumanogoh A, Yoshida M, Mochizuki H, Kuwabara S, Yamashita T (2011) RGMa modulates T cell responses and is involved in autoimmune encephalomyelitis. Nature medicine 17:488-494.

Niederkofler V, Salie R, Sigrist M, Arber S (2004) Repulsive guidance molecule (RGM) gene function is required for neural tube closure but not retinal topography in the mouse visual system. The Journal of neuroscience : the official journal of the Society for Neuroscience 24:808-818.

Nohra R, Beyeen AD, Guo JP, Khademi M, Sundqvist E, Hedreul MT, Sellebjerg F, Smestad C, Oturai AB, Harbo HF, Wallstrom E, Hillert J, Alfredsson L, Kockum I, Jagodic M, Lorentzen J, Olsson T (2010) RGMA and IL21R show association with experimental inflammation and multiple sclerosis. Genes and immunity 11:279-293.

Olanow CW, Stern MB, Sethi K (2009) The scientific and clinical basis for the treatment of Parkinson disease (2009). Neurology 72:S1-136.

Paxinos AFKBJ (2001) The Mouse Brain in Stereotaxic Coordinates: Academic Press, New York.

Perez XA, Parameswaran N, Huang LZ, O'Leary KT, Quik M (2008) Pre-synaptic dopaminergic compensation after moderate nigrostriatal damage in non-human primates. Journal of neurochemistry 105:1861-1872.

Reynolds AD, Stone DK, Hutter JA, Benner EJ, Mosley RL, Gendelman HE (2010) Regulatory T cells attenuate Th17 cell-mediated nigrostriatal dopaminergic neurodegeneration in a model of Parkinson's disease. Journal of immunology 184:2261-2271.

Rodriguez A, Pan P, Parkkila S (2007) Expression studies of neogenin and its ligand hemojuvelin in mouse tissues. The journal of histochemistry and cytochemistry : official journal of the Histochemistry Society 55:85-96.

Roghani M, Behzadi G, Baluchnejadmojarad T (2002) Efficacy of elevated body swing test in the early model of Parkinson's disease in rat. Physiology & behavior 76:507-510.

Samad TA, Srinivasan A, Karchewski LA, Jeong SJ, Campagna JA, Ji RR, Fabrizio DA, Zhang Y, Lin HY, Bell E, Woolf CJ (2004) DRAGON: a member of the repulsive guidance molecule-related family of neuronal- and muscle-expressed membrane proteins is regulated by DRG11 and has neuronal adhesive properties. The Journal of neuroscience : the official journal of the Society for Neuroscience 24:2027-2036.

Schintu N, Frau L, Ibba M, Caboni P, Garau A, Carboni E, Carta AR (2009) PPAR-gamma-mediated neuroprotection in a chronic mouse model of Parkinson's disease. The European journal of neuroscience 29:954-963.

1035 Schwab JM, Conrad S, Monnier PP, Julien S, Mueller BK, Schluesener HJ (2005a) Spinal
1036 cord injury-induced lesional expression of the repulsive guidance molecule (RGM).
1037 The European journal of neuroscience 21:1569-1576.
1038 Schwab JM, Monnier PP, Schluesener HJ, Conrad S, Beschorner R, Chen L, Meyermann R,
1039 Mueller BK (2005b) Central nervous system injury-induced repulsive guidance
1040 molecule expression in the adult human brain. Archives of neurology 62:1561-1568.
1041 Shabanzadeh AP, Tassew NG, Szydlowska K, Tymianski M, Banerjee P, Vigouroux RJ,
1042 Eubanks JH, Huang L, Geraerts M, Koeberle PD, Mueller BK, Monnier PP (2015)
1043 Uncoupling Neogenin association with lipid rafts promotes neuronal survival and
1044 functional recovery after stroke. Cell death & disease 6:e1744.
1045 Smith GA, Rocha EM, Rooney T, Barneoud P, McLean JR, Beagan J, Osborn T, Coimbra M,
1046 Luo Y, Hallett PJ, Isacson O (2015) A Nurr1 agonist causes neuroprotection in a
1047 Parkinson's disease lesion model primed with the toll-like receptor 3 dsRNA
1048 inflammatory stimulant poly(I:C). PloS one 10:e0121072.
1049 Srinivasan BS, Doostzadeh J, Absalan F, Mohandessi S, Jalili R, Bigdeli S, Wang J,
1050 Mahadevan J, Lee CL, Davis RW, William Langston J, Ronaghi M (2009) Whole
1051 genome survey of coding SNPs reveals a reproducible pathway determinant of
1052 Parkinson disease. Human mutation 30:228-238.
1053 Sutherland GT, Matigian NA, Chalk AM, Anderson MJ, Silburn PA, Mackay-Sim A, Wells
1054 CA, Mellick GD (2009) A cross-study transcriptional analysis of Parkinson's disease.
1055 PloS one 4:e4955.
1056 Tagliaferro P, Burke RE (2016) Retrograde Axonal Degeneration in Parkinson Disease.
1057 Journal of Parkinson's disease 6:1-15.
1058 Tanabe S, Yamashita T (2014) Repulsive guidance molecule-a is involved in Th17-cell-
1059 induced neurodegeneration in autoimmune encephalomyelitis. Cell reports 9:1459-
1060 1470.
1061 Tassew NG, Charish J, Seidah NG, Monnier PP (2012) SKI-1 and Furin generate multiple
1062 RGMa fragments that regulate axonal growth. Developmental cell 22:391-402.
1063 Tillerson JL, Miller GW (2003) Grid performance test to measure behavioral impairment in
1064 the MPTP-treated-mouse model of parkinsonism. Journal of neuroscience methods
1065 123:189-200.
1066 Ulusoy A, Sahin G, Bjorklund T, Aebischer P, Kirik D (2009) Dose optimization for long-
1067 term rAAV-mediated RNA interference in the nigrostriatal projection neurons.
1068 Molecular therapy : the journal of the American Society of Gene Therapy 17:1574-
1069 1584.
1070 Van Battum EY, Brignani S, Pasterkamp RJ (2015) Axon guidance proteins in neurological
1071 disorders. The Lancet Neurology 14:532-546.
1072 van den Heuvel DM, Hellemons AJ, Pasterkamp RJ (2013) Spatiotemporal expression of
1073 repulsive guidance molecules (RGMs) and their receptor neogenin in the mouse brain.
1074 PloS one 8:e55828.
1075 Wilson NH, Key B (2007) Neogenin: one receptor, many functions. The international journal
1076 of biochemistry & cell biology 39:874-878.
1077 Yamada T, McGeer PL, Baimbridge KG, McGeer EG (1990) Relative sparing in Parkinson's
1078 disease of substantia nigra dopamine neurons containing calbindin-D28K. Brain
1079 research 526:303-307.
1080 Yamashita T, Mueller BK, Hata K (2007) Neogenin and repulsive guidance molecule
1081 signaling in the central nervous system. Current opinion in neurobiology 17:29-34.
1082 Yang C, Hao F, He J, Lu T, Klein RL, Zhao LR, Duan WM (2016) Sequential Adeno-
1083 Associated Viral Vector Serotype 9-Green Fluorescent Protein Gene Transfer Causes

1084 Massive Inflammation and Intense Immune Response in Rat Striatum. Human gene
1085 therapy.
1086 Yoshida J, Kubo T, Yamashita T (2008) Inhibition of branching and spine maturation by
1087 repulsive guidance molecule in cultured cortical neurons. Biochemical and
1088 biophysical research communications 372:725-729.
1089 Zolotukhin S, Byrne BJ, Mason E, Zolotukhin I, Potter M, Chesnut K, Summerford C,
1090 Samulski RJ, Muzyczka N (1999) Recombinant adeno-associated virus purification
1091 using novel methods improves infectious titer and yield. Gene therapy 6:973-985.
1092
1093
1094

Figure legends

Figure 1. RGMa is expressed in human dopaminergic neurons in the substantia nigra of both control subjects and Parkinson's disease patients. A-C. *In situ* hybridization for human RGMa mRNA (blue staining) is exclusively present in cellular structures morphologically identified as neurons (large cells with a nucleolus in the center of the nucleus) in a control (**A**) and PD patient (**B**). Note the absence of staining in the sense probe (**C**). Most neurons contained neuromelanin (brown pigmentation) indicating their DA phenotype (best visible in panel **C**). Sections were used from the following NBB donors: control 00-049 (**A**), PD 02-064 (**B**), control 00-050 (**C**). Scale bar represents 0.1 mm. **D-E.** Immunofluorescent staining for RGMa protein (red; antibody SC-46482) in the SN of control (**D**) and PD (**E**) brains is mainly localized to DA neurons counterstained for TH (green). Arrows point to TH positive neurons also positive for punctate RGMa protein expression. Sections were used from NBB donors: control 98-126 and PD 00-115. **F-G.** Immunohistochemical staining for RGMA protein (red) and its receptor Neogenin (green) in control (**F**) and PD (**G**) SN tissue. Arrows point to Neogenin positive neurons also showing punctate RGMa protein expression. Sections were used from NBB donors: control 00-142 and PD 02-003. Scale bar represents 20µm.

Figure 2. AAV vectors direct RGMa expression and secretion in a neuronal cell line and dose dependent expression in the mouse brain. A. AAV plasmid-mediated overexpression of mouse RGMa in N2A cells results in the production and secretion of RGMa protein. N2A cells were either untreated (UnTr) or transfected with the expression plasmids pAAV-SYN-GFP or pAAV-SYN-mRGMa. Anti-mouse RGMa antibody (R&D AF2458) was used to detect mouse RGMa protein in the cell lysate (LYS samples) or the culture medium (MED samples) 3 days after transfection. N2A cells produce mouse RGMa after transfection of the expected molecular weight: multiple bands are visible around 49-55 kDa representing the full-length form, and one prominent band at 33kDa representing the cleaved membrane bound C-terminal form. RGMa is also release from the transfected N2A cells, which results in the N-terminal 30kDa form of RGMa in the medium samples. β-actin was used as loading control. **B.** Comparison of RGMa protein levels in the SN of mouse injected with a high titer ($9.0x10^{12}$ gc/ml) and low titer ($3.0x10^{12}$ gc.ml). The RGMa fluorescence was twice as high in the high titer injected mice compared to the low titer injected mice ($p< 0.0001$, $F (3, 22) = 41.21$). Data is represented in percentages of RGMa fluorescence levels relative to the AAV-Empty RGMa. Tissue from 6 mice was quantified in the high titer treatment group, and from 7 mice in low titer treatment group. Example images used for the quantification of RGMa are shown in Figure 6B (high dose experiment) and 7B (low dose experiment). Statistical analysis was performed using one way ANOVA with Tukey's post hoc multiple testing correction, **** $p<0.0001$.

Figure 3. AAV vectors drive RGMa expression and secretion in the mouse brain. A. Quantification of the percentage of RGMa fluorescence intensity in SN and the striatum of the bilateral and unilateral high titer injected animals. RGMa protein levels were significantly increased in the injected SN compared to AAV-Empty injected ($p<0.0001$) and non-injected SN ($p=0.003$). Similarly, striatal RGMa levels were significantly higher in the bilaterally AAV-

RGMa injected animals compared to the AAV-Empty injected animals ($p<0.0001$) and in the ipsilateral striatum versus the contralateral striatum of the unilaterally AAV-RGMa injected animals ($p=0.0126$). **B.** Quantification of RGMA fluorescence intensity in SN and striatum in low titer AAV-RGMa injected animals. The percentage of RGMa fluorescence intensity were significantly increased in the right SN injected with AAV-RGMa and, to a smaller extent, in the left non- injected SN, compared to all control groups (GFP, Saline or Empty, SN right $p< 0.0001$, $F (3, 25) = 159.0$, SN left $p< 0.0001$, $F (3, 25) = 42.9$). Both striatal ($p=0.001$) and SN ($p=0.0001$) levels of RGMa were significantly higher on the right transduced side of the nigrostriatal tract. Data is represented in percentages of fluorescence relative to the AAV-Empty RGMa fluorescence. For representative images of the RGMa immunohistochemical stained mouse SN and striatum see Figure 6B and 6E and Figure 7B and 7E. Tissue from 6 mice was measured in the high titer treatment group, and from 7 mice in low titer treatment group. Statistical analysis was performed using student T test and one way ANOVA with Tukey's post hoc multiple testing correction, * $p< 0.05$, ** $p< 0.01$, *** $p<0.001$, **** $p<0.0001$

Figure 4. High dose AAV-mediated overexpression of RGMa in the mouse SN results in a progressive and severe induction of motor deficits. A. Grid test performance showed a progressive increase of front paw placement errors in both unilateral (red) and bilateral (purple) RGMa overexpressing mice when compared to the AAV-Empty injected animals (blue) ($p<0.0001$, $F (2,270) = 49.97$). Starting at week 2.5 post-surgery RGMa overexpressing mice displayed significantly higher error rates compared to the control with variations at different time points (see colored asterisks, explained below) **B.** Hind limb placement measurements on the narrow beam test showed significant increase in the number of hind paw placement errors between the injection groups ($p<0.0001$, $F (2,270) = 46.52$) with post-hoc test indicating unilaterally RGMa injected mice to develop an increase in hind limb slips compared to the AAV-Empty injected animals (red asterisks). **C.** Preference of bilateral or unilateral front paw use was measured by a cylinder test. The ratio of single right paw use during rearing over total rearing events was determined ($p<0.0001$, $F (2,240) = 46.96$). Both bilateral and unilateral RGMa overexpressing mice showed increased right paw use at different time points compared to the AAV-Empty control group. **D.** The swing test revealed a significant difference between the injected groups ($p<0.0001$, $F (2,195) = 57.19$), with an increase in the rotation preference towards the left in animals injected unilaterally with AAV-RGMa when compared to AAV-Empty animals. Animals receiving a bilateral injection of AAV-RGMa or AAV-Empty did not develop a swing preference over time. **E.** Increased events of tremor were observed during the time of the experiment in the RGMa overexpressing mice ($p<0.0001$, $F (2,240) = 55.58$), with both uni- and bilaterally injected RGMa animals compared to the AAV-Empty injected animals starting from week 4.5 onwards. **F**. Mice bilaterally overexpressing RGMa showed a significant decrease in body weight towards the end of the experiment ($p<0.0001$, $F (2,360) = 42.86$). For all tests, week 0 is the baseline measurement performed 2 days before the AAV injection. Each treatment group consists of 6 animals. Statistical analysis was performed with a two way ANOVA with Tukey's post hoc multiple testing correction, * $p< 0.05$, ** $p< 0.01$, *** $p<0.001$, **** $p<0.0001$. Within each panel different colored asterisks denote significance between different treatment groups compared to the AAV-Empty group: black asterisks- both RGMa groups, red asterisks -unilateral RGMa group, purple asterisks -bilateral RGMa group.

Figure 5. Low dose AAV-mediated overexpression of RGMa in the mouse SN results in a mild but progressive induction of motor behavioral deficits. A. A significant increase in front paw placement errors was observed in the grid test in the RGMa group (red) compared to the three control groups (AAV-Empty (blue), AAV-GFP (green) and saline (black)) ($p<0.0001$, $F(3,400) = 61.31$). Post hoc testing showed an increase in error rates in RGMa overexpressing mice from week 3.5 post surgery compared to all three control groups (black asterisks) with some variation at different testing time points (red asterisks). **B.** Hind limb placement was measured by the narrow beam test. Mice treated with AAV-RGMa showed small but significant increased error rate in this test compared to the controls ($p=0.0002$, $F(3,416) = 6.586$). **C.** Preference of bilateral or unilateral front paw use was measured in a cylinder test. The ratio of right paw use over total rearing events was determined. RGMa overexpressing mice progressively increased their preference for only right paw use compared to control groups ($p<0.0001$, $F(3,375) = 12.37$). Post hoc testing indicated more right paw use in RGMa animals compared to either one or two control treatment groups (red asterisks) or to all control groups (black asterisk) starting from week 8 post surgery. **D.** The swing test revealed no significant differences in the rotation preference of the mice between any of the treatment groups. **E.** Tremor was observed in RGMa overexpressing mice ($p<0.0001$, $F(3,416) = 20.71$) starting 3.5 weeks post-surgery. **F**. None of the treatment groups showed any significant differences in weight gain. For all tests, week 0 is the baseline measurement performed 2 days before the AAV injection. Each treatment group includes 8 animals per quantification, with the saline group containing 6 animals. Statistical analysis was performed with a two way ANOVA with Tukey's post hoc multiple testing correction, * $p< 0.05$, ** $p< 0.01$, *** $p<0.001$, **** $p<0.0001$.

Figure 6. High dose AAV-mediated overexpression of RGMa in the mouse SN induces a decline in the number of DA neurons and affects TH expression in the surviving neurons. A. Quantification of the neuronal density in the SN in AAV-Empty (bilateral), AAV-RGMa (unilateral) and AAV-RGMa (bilateral) injected SN. Bilateral RGMa overexpression resulted in a decrease in both the total (24%, $p=0.0136$) and tyrosine hydroxylase positive (TH+) (38%, $p=0.012$) neuronal density in the SN compared to the AAV-Empty bilateral injected SN (total SN neuron count combined from both SN). Unilateral AAV-RGMa-mediated overexpression also induced a significant decrease in total number of neurons (18%, $p=0.004$) and in TH+ neurons (40%, $p=0.0072$) in the right injected SN compared to the left, non-injected SN. Other (TH-) neuronal profiles were not affected by RGMa overexpression. **B.** Immunohistochemical staining for TH (green), GFAP (red) and RGMa (blue) in mouse SN injected with AAV-Empty (bilateral), AAV-RGMA (unilateral) and AAV-RGMA (bilateral). **C.** Quantification of TH fluorescence positive area in the SN. Bilateral overexpression of RGMa in the SN is associated with a decrease of TH+ area in the SN compared to bilateral AAV-Empty injected SN ($p=0.0005$, values from both left and right SN are pooled). TH fluorescence area in the right SN of animals unilaterally injected with AAV-RGMa is also decreased when compared to the left, non-injected SN ($p=0.0026$). **D.** Quantification of TH fluorescence levels in the SN. Despite the TH+ neuronal loss, TH fluorescence intensity is not significantly different in the SN of animals bilaterally injected with AAV-RGMa compared to the AAV-Empty injected animals ($p=0.1261$). In the unilaterally AAV-RGMa injected animals, the left, non-injected SN shows a significant increase in TH fluorescence intensity when compared to the right injected SN ($p=0.006$), suggesting a compensatory mechanism. **E.** Immuno-histochemical staining for TH (green), GFAP (red)

and RGMa (blue; antibody SC-46482) in the striatum following the transduction of the SN with AAV-Empty (bilateral), AAV-RGMa (unilateral) and AAV-RGMa (bilateral). RGMa protein is shown to be transported from the transduced SN to the nigrostriatal projection target sites in the striatum. **F.** Quantification of TH fluorescence levels in the striatum. Overexpression of RGMa in the SN is associated with a decrease in TH fluorescence intensity in the striatum in bilateral RGMa injection paradigm compared to the AAV-Empty injected animals ($p=0.0085$). Similarly, the striatal TH intensity levels are decreased in the right striatum of the right SN injected animals compared to the left striatum ($p=0.0004$). Each treatment group includes 6 animals per quantification. Statistical analysis was performed using student T test, * $p< 0.05$, ** $p< 0.01$, *** $p<0.001$, **** $p<0.0001$. Scale bar for B represents 0.25 mm and for E is 0.5 mm.

Figure 7. Low dose AAV-mediated overexpression of RGMa induced a decline in DA neurons and increase in TH protein levels indicative of a compensation mechanism. **A.** Quantification of the neuronal density in AAV-Empty, AAV-GFP and AAV-RGMa injected and non-injected SN. RGMa overexpression resulted in a decrease in both the total (23 and 26%) and tyrosine hydroxylase (TH) positive (30 and 33%) neuronal density in the AAV-RGMa injected SN compared to the AAV-Empty and AAV-GFP injected SN (total neurons: $p=0.0015$, $F (2, 19) = 9.318$, TH neurons: $p=0.0041$, $F (2, 19) = 7.449$). TH-negative neurons were generally not affected by RGMa overexpression, with an exception when comparing to AAV-GFP injected SN ($p=0.0488$, $F (2, 19) = 3.555$). Total and TH+ neuronal density was significantly decreased in the AAV-RGMa injected SN compared to the not injected SN ($p=0.0029$, $p=0.0018$ respectively). **B.** Immunohistochemical staining for TH (red), GFP (green) and RGMa (blue) in the SN injected with Saline, AAV-Empty, AAV-GFP or AAV-RGMA virus. **C.** Quantification of TH+ area in the SN. The TH+ area was significantly decreased in the SN injected with AAV-RGMa compared to all control groups ($p=0.0012$, $F (3, 21) = 7.692$) as well as to the contralateral (non-injected) SN of the RGMa-treated animals ($p=0.0048$). **D.** Quantification of TH fluorescence levels in the SN. Overexpression of RGMa in the SN is associated with an increase in TH fluorescence in the non-injected contralateral SN compared to all control groups ($p=0.0006$, $F (3, 23) = 8.3$). TH fluorescence intensity in the AAV-RGMa injected SN is not altered compared to the control treatment groups. **E.** Immunohistochemical staining for TH (red), GFP (green) and RGMa (blue; antibody SC-46482) in the striatum following the transduction of the SN with AAV-GFP or AAV-RGMa. Note that both GFP and RGMa protein is transported from the injected (right) SN to the nigrostriatal projection target sites in the right striatum. **F.** Quantification of TH fluorescence intensity in the striatum. Overexpression of RGMa in the SN is associated with an increase in TH fluorescence intensity in the left contralateral striatum compared to the AAV-GFP control striatum ($p=0.0082$) and compared to the right AAV-RGMa striatum ($p=0.0037$). TH fluorescent levels in the right striatum were not different in AAV-RGMa group compared to all three control treatment groups ($p=0.6139$). Each treatment group includes 8 animals per quantification, with the saline group containing 6 animals. Statistical analysis was performed using one way ANOVA with Tukey's post hoc multiple testing correction and student T test, * $p< 0.05$, ** $p< 0.01$, *** $p<0.001$, **** $p<0.0001$. Scale bar for figure B represents 0.25 mm and for figure E represents 0.5 mm.

Figure 8. High dose AAV-mediated overexpression of RGMa in the mouse SN induced a gliotic response. A. Immunohistochemical staining for tyrosine hydroxylase (TH, green) and Iba1 (red) in the SN injected with high titer AAV-Empty bilateral, AAV-RGMa unilaterally and AAV-RGMa bilaterally. Scale bar represents 0.25 mm. **B.** Quantification of fluorescence signal in the SN of mice receiving a unilateral injection of high titer AAV-RGMa. GFAP and Iba1 fluorescence intensities are increased in the AAV-RGMa injected (right) SN compared to the non-injected (left) SN. **C.** Quantification of fluorescence signal in the SN of mice receiving a bilateral injection of high titer AAV-Empty or the AAV-RGMa viral vector. GFAP and Iba1 intensities are increased in the AAV-RGMa injected SN compared with the AAV-Empty injected animals. Fluorescence intensities from right and left SN were averaged across both SN to provide the total fluorescence intensity per entire SN in each bilateral AAV treatment. **D.** Quantification of fluorescence signal in the striatum of mice receiving a unilateral injection of high titer AAV-RGMa in the SN. GFAP fluorescence intensity is slightly decreased in the right (injected) striatum compared to the left ($p=0.027$). We observed no differences in Iba1 levels between the two hemispheres. **E.** Quantification of fluorescence signal in the striatum of mice receiving a bilateral injection of high titer AAV-Empty or AAV-RGMa virus in the SN. We observed no differences in GFAP fluorescence intensities between the two groups. Iba1 fluorescence intensity is slightly decreased in the striatum of AAV-RGMa injected mice compared to the AAV-Empty injected animals ($p=0.015$). Fluorescence intensities from right and left striata were averaged across both striata to provide the total fluorescence intensity per AAV treatment. Each treatment group includes 6 animals per quantification. Statistical analysis was performed using student T test, * $p< 0.05$, ** $p< 0.01$, *** $p<0.001$.

Figure 9. Low dose AAV-mediated overexpression of RGMa induced a gliotic response. A. Immunohistochemical staining for tyrosine hydroxylase (TH, green), GFAP (red) and Iba1 (blue) in mouse SN injected with saline, AAV-Empty, AAV-GFP or AAV-RGMA. The two panels represent the injected and non-injected SN for each animal. Due to a limitation of the available number of fluorescence channels, two series of SN tissue were used for animals injected with AAV-GFP i.e., one to stain for GFAP and one to stain for Iba1. **B.** Quantification of GFAP fluorescence signal in the SN 12 weeks post injection. Overexpression of RGMa in the SN is associated with an increase in GFAP fluorescence intensity in the injected SN compared to AAV-GFP group ($p=0.0020$, $F(3, 25) = 6.583$) and to the non-injected SN in AAV-RGMa treated animals ($p<0.0001$). GFAP fluorescence is decreased in the non-injected SN of AAV-GFP treated animals compared to the non-injected SN of the AAV-RGMa, AAV-Empty and saline treated groups ($p<0.0001$, $F(3, 25) = 32.97$). **C.** Quantification of Iba1 fluorescence signal in the SN 12 weeks post injection. Overexpression of RGMa in the SN is associated with an increase in Iba1 fluorescence intensity in the injected SN compared to the contralateral non-injected SN in RGMA treated animals ($p<0.0001$), as well as to the injected SN of the AAV-Empty and saline treated animals ($p<0.0001$, $F(3, 25) = 19.66$). Iba1 fluorescence is significantly increased in both SN of animals injected with AAV-GFP compared with both SN of AAV-RGMa, AAV-Empty and saline treated animals (not injected SN $p<0.0001$, $F(3, 25) = 35.26$, injected SN $p<0.0001$, $F(3, 25) = 19.66$). AAV-RGMa treatment group consists of 7 animals, AAV-GFP and AAV-Empty consist of 8 animals per group and the saline treatment group contains 6 animals. Statistical analysis was performed using one way ANOVA with Tukey's post hoc multiple

testing correction and student T test, * p< 0.05, ** p< 0.01, *** p<0.001, **** p<0.0001. Scale bars represent 0.25 mm.

Figure 10. Akt and pAkt levels in SN DA neurons upon high dose RGMa overexpression. A. Quantification of Akt and pAkt fluorescence signal in the SN DA neurons. Overexpression of RGMa in the SN is not associated with an increase in either the total Akt or the Ser473 phosphorylated Akt (pAkt) fluorescence intensity in the DA neurons of the AAV-RGMa injected animals compared to AAV-Empty group (p=0.174 and p=0.333 respectively). Total Akt analysis was performed on 5 animals per experimental group. PhosphoAkt analysis was performed on 5 animals in the AAV-Empty injected group and 4 animals in the AAV-RGMa injected group. **B.** Quantification of pAkt fluorescence signal in the SN DA neurons corrected for the total Akt signal. Overexpression of RGMa in the SN is not associated with an increase in pAkt fluorescence intensity in the DA neurons of the AAV-RGMa injected animals compared to AAV-Empty group (p=0.895). PhosphoAkt analysis was performed on 5 animals in the AAV-Empty injected group and 4 animals in the AAV-RGMa injected group. Statistical analysis was performed using student T test.

Tables

Subject	Diagnosis	Sex	Age	PMI	pH	BW	RIN		Cause of Death
00-115	PD/DEM	M	70	9:05	6.33	1258	6.2		Pneumonia, septic shock
04-045	PD/DEM	M	71	6:58	6.55	1358	8.4	*	Pneumonia
00-139	PD/DEM	M	72	7:15	6.55	1546	6.7		Uremia
02-003	PD	F	75	5:00	6.52	1218	9.6	*	Euthanasia
02-011	PD	F	79	5:45	6.37	1203	8.7	*	Myocard Infraction
00-034	PD	M	86	8:30	6.52	1178	9.2	*	Unknown
02-064	PD	M	87	7:20	6.37	1166	7.4		Respiratory insufficiency
98-126	CTRL	M	71	6:00	6.54	1385	8.8		Respiratory insufficiency
00-049	CTRL	M	78	6:55	6.42	1332	9.2	*	Cardiac failure
97-144	CTRL	M	78	4:00	6.43	1160	9	*	Pulmonary carcinoma
00-142	CTRL	F	82	5:30	6.60	1280	9.2	*	Myocardial infarct
00-022	CTRL	F	83	7:45	6.52	1102	9.2	*	Acute myocard infraction
98-062	CTRL	M	85	4:35	6.95	1332	7.5		Respiratory insufficiency
99-046	CTRL	F	89	5:10	6.62	1168	9.5		Cardiac arrest
01-029	CTRL	F	90	5:25	6.58	1066	7.6		Myocard infraction
00-050	CTRL	F	52	6:50	7.16	1258	_		Leiomyosarcoma with metastasis

Table 1. Clinicopathological data of human post-mortem tissue samples used for in-situ hybridization and immunohistochemistry. All brain tissue was collected from donors from whose written informed consent for a brain autopsy and the use of the material and clinical information for research purposes had been obtained by the NBB. For further diagnosis, an extensive neuropathological investigation was performed on all PD and control tissue. Control tissue did not present any Braak pathology score for neurofibrillary tangles higher than 2 (Braak et al., 2003) and neither control nor PD subject had a known history of neurological or psychiatric disease other than PD or PD-related dementia. All PD patients received dopamine replacement therapy during the course of the disease. Column 'Subjects' provides the NBB numbers of each donor. Abbreviations: PD- Parkinson's disease; CTRL-control; PD/DEM- Parkinson's disease with dementia; PMI- post-mortem interval (hours); m-male; f- female; BW- brain weight (grams); RIN- RNA integrity number. Samples marked with an * have been used in the microarray study and all samples (except case 00-050) were used for qPCR analysis as described earlier (Bossers et al., 2009). Donor NBB 00-050 was only used for in situ hybridizations.

	Low dose RGMa overexpression	**Low dose RGMa overexpression**
Virus	AAV2/7-RGMa, AAV2/7-Empty, AAV2/7-GFP, Saline	AAV2/7-RGMa unilateral, AAV2/7-RGMa bilateral, AAV2/7-Empty
Titer	3.0x10^12	9.0x10^12
Number of animals per group	N=8, for saline N=6	N=6
Survival time	12 weeks	18.5 weeks

Table 2. Description of the experimental animal groups, the viral vectors used and the viral vector dose injected in the two overexpression experiments.

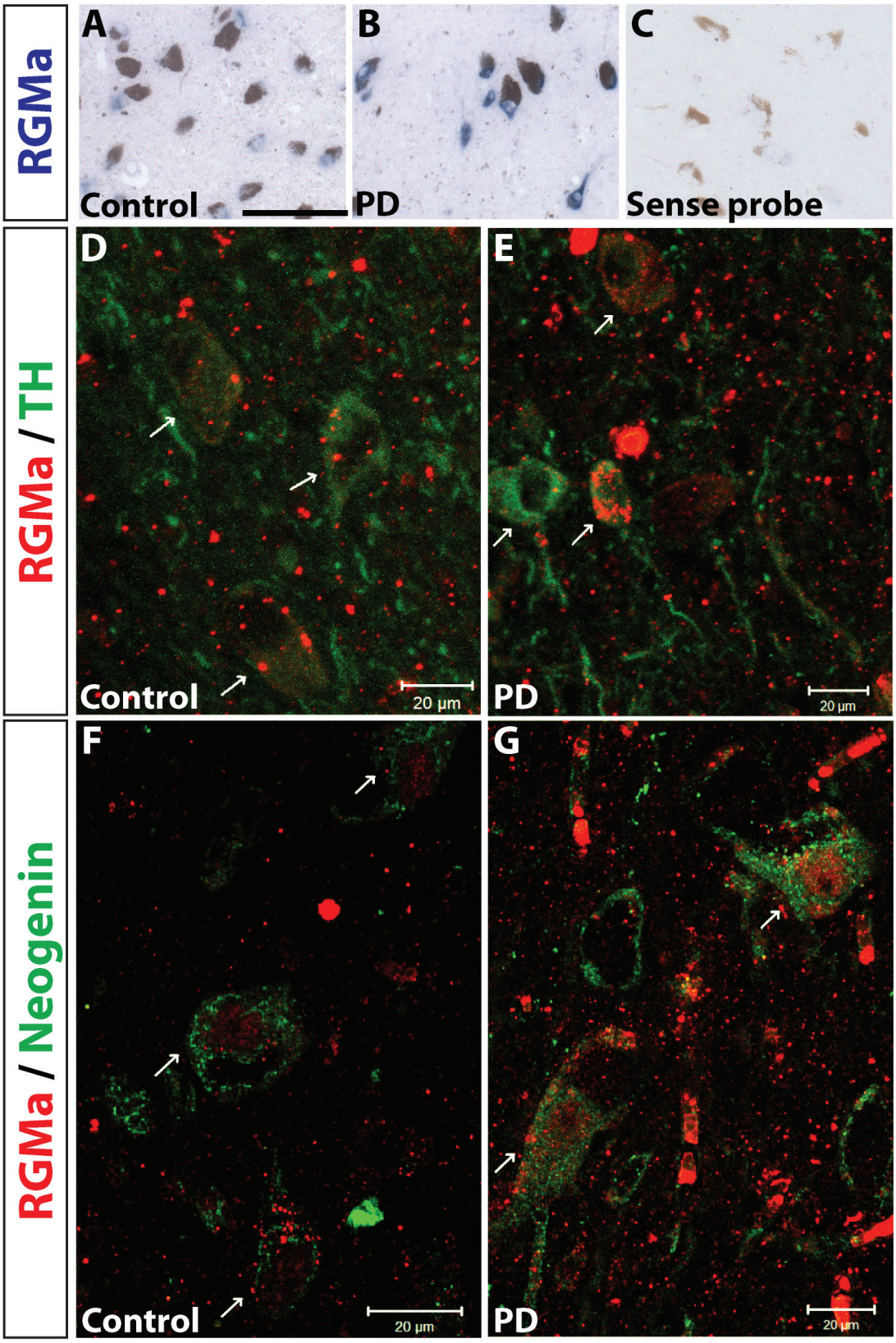

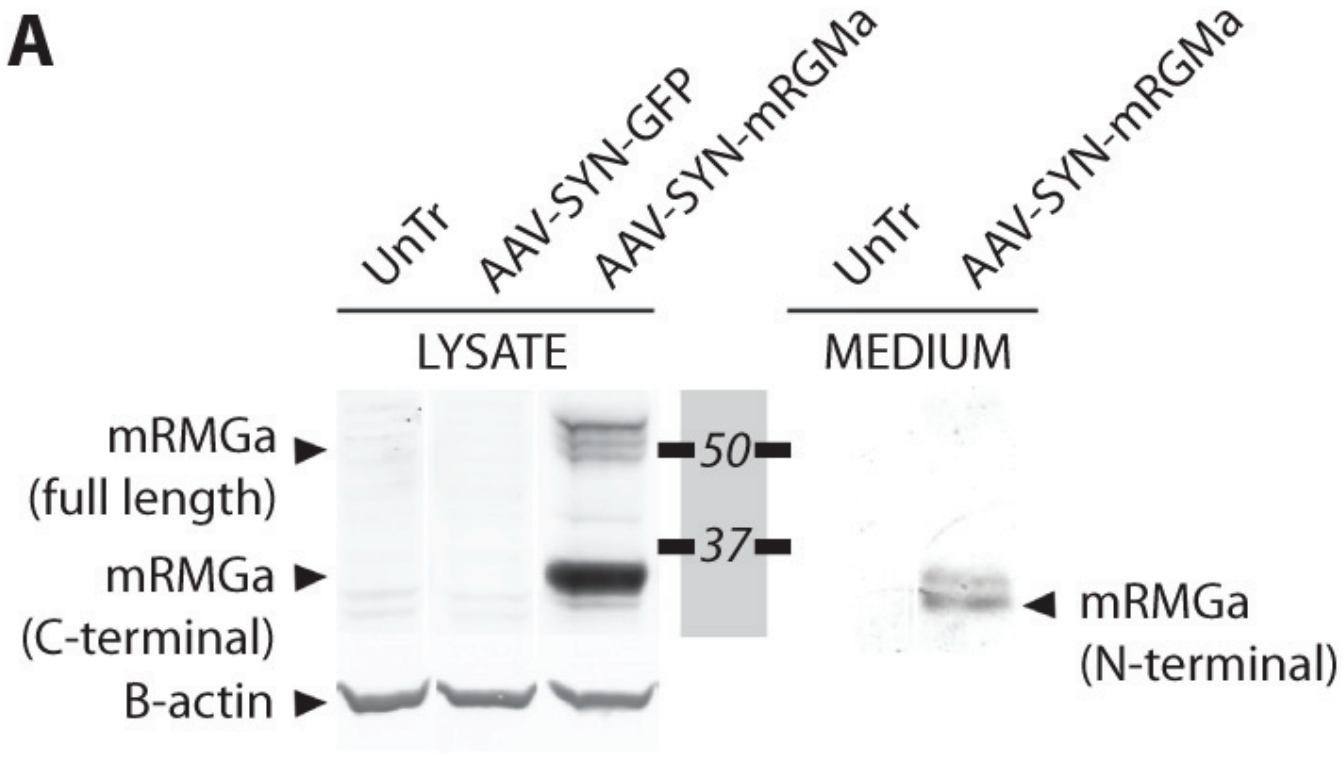

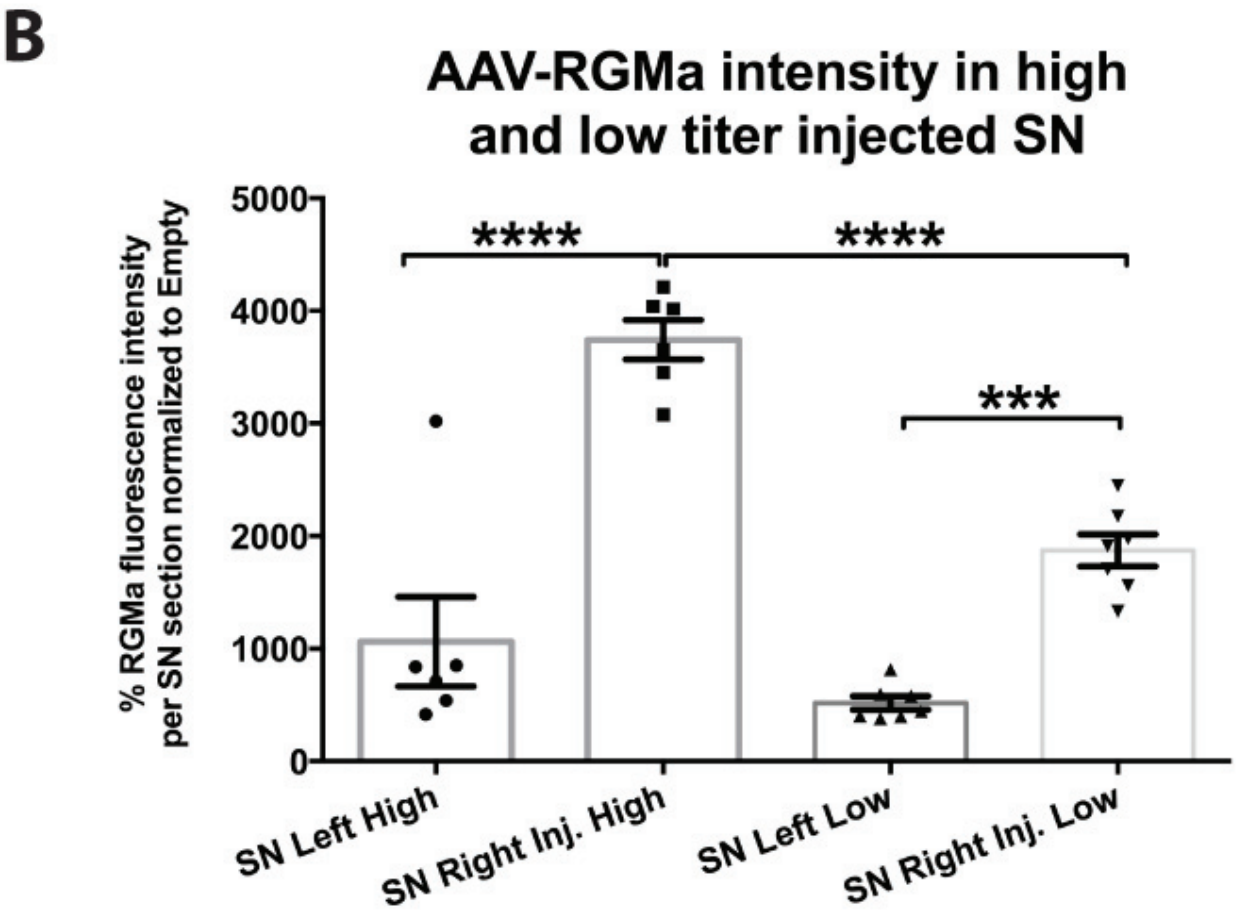

A

RGMa fluorescence levels in high titer injected animals

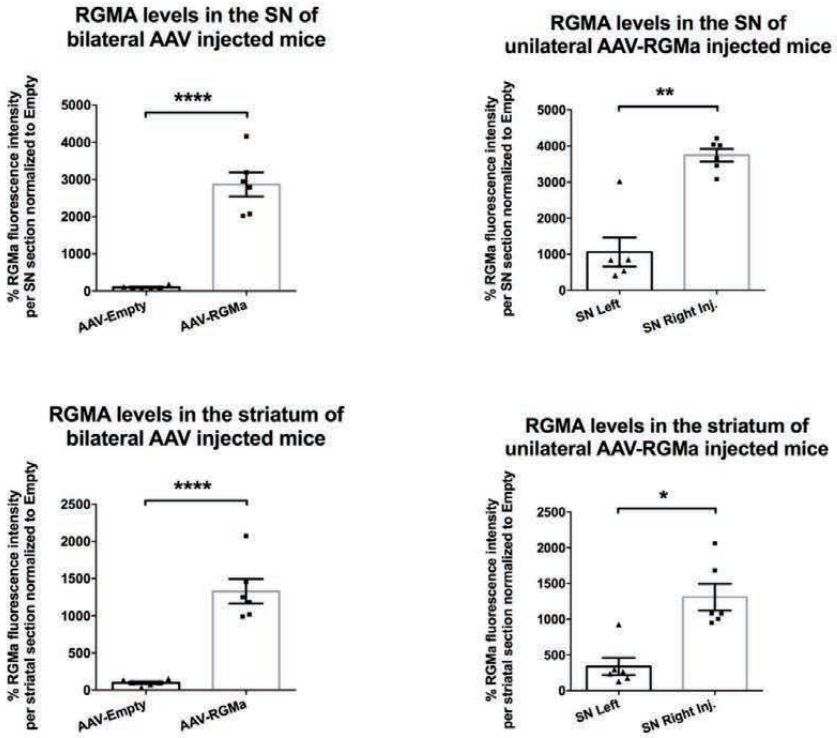

B

RGMa fluorescence levels in low titer injected animals

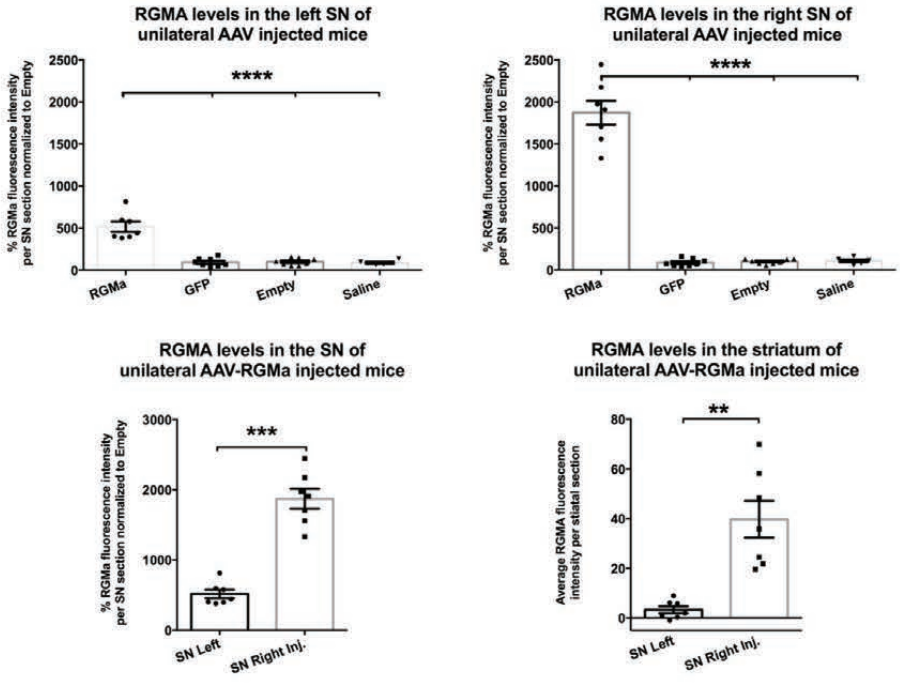

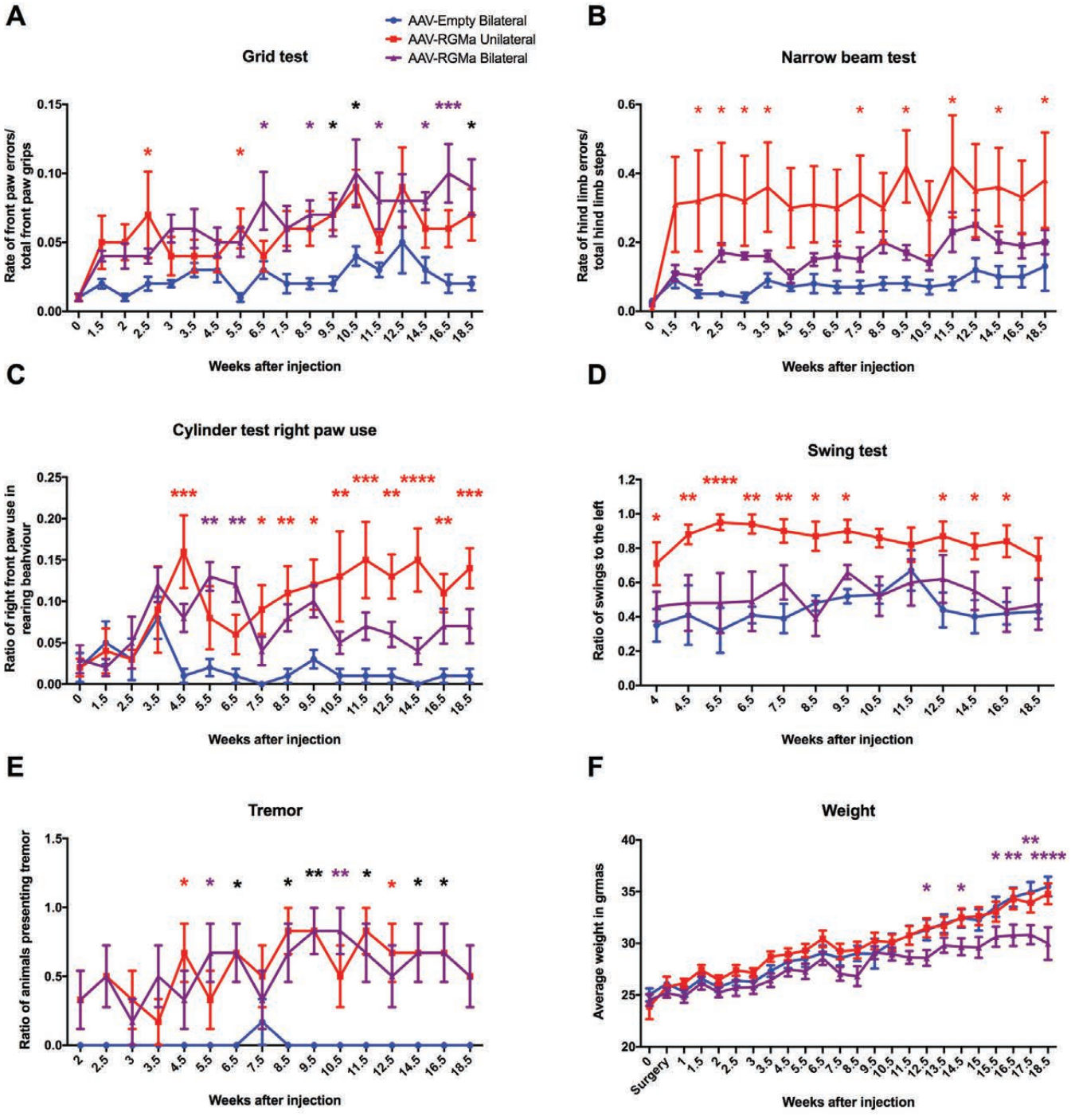

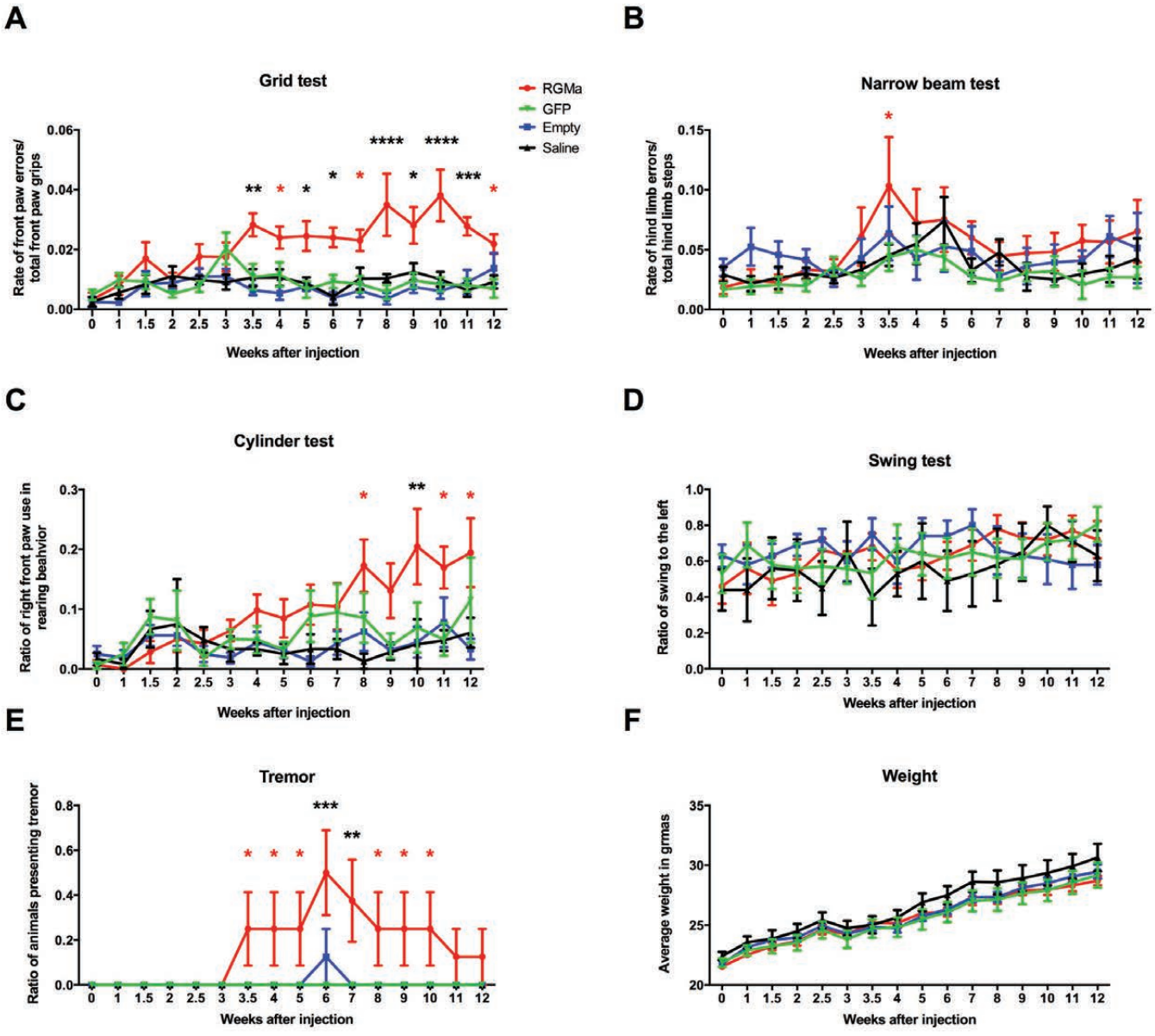

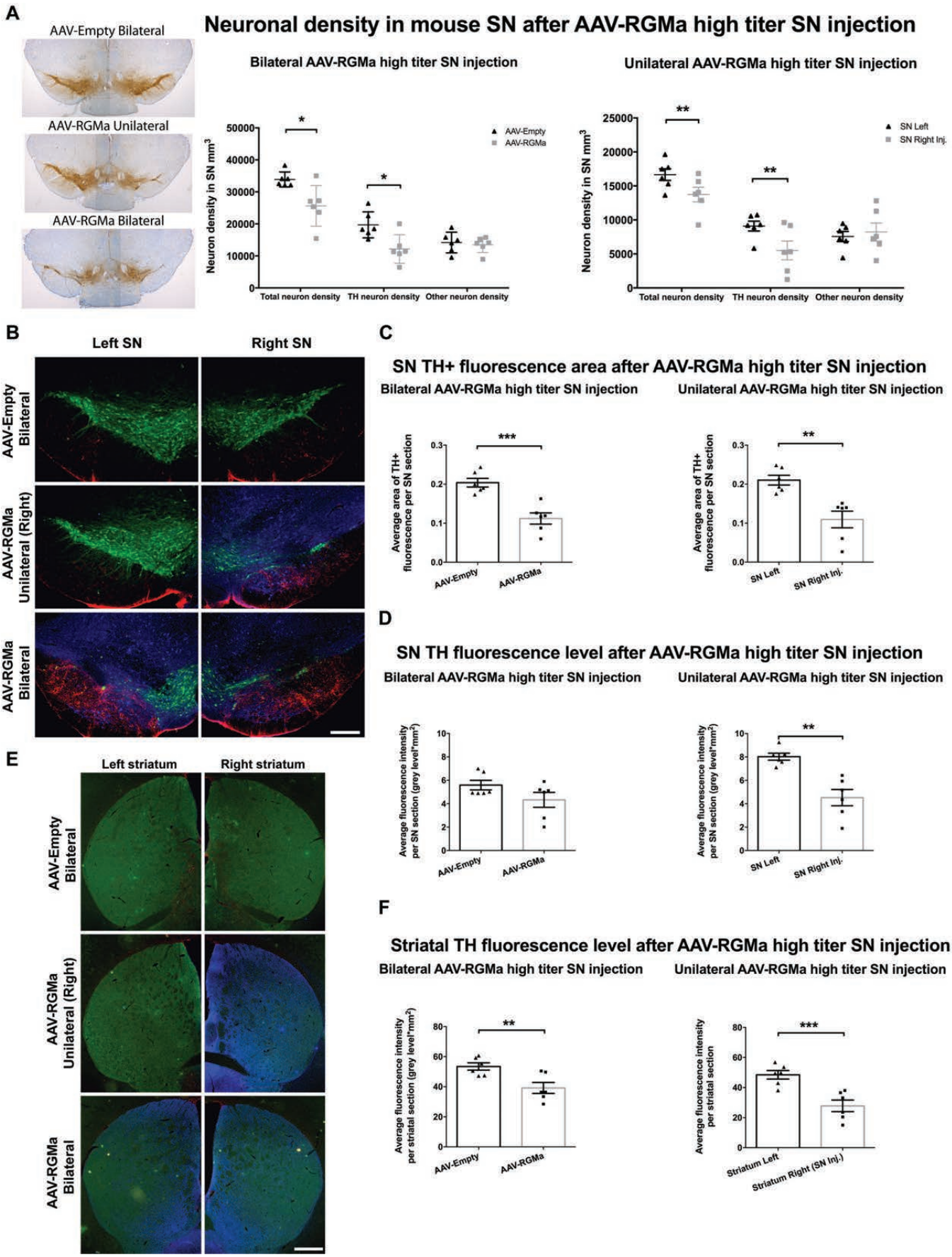

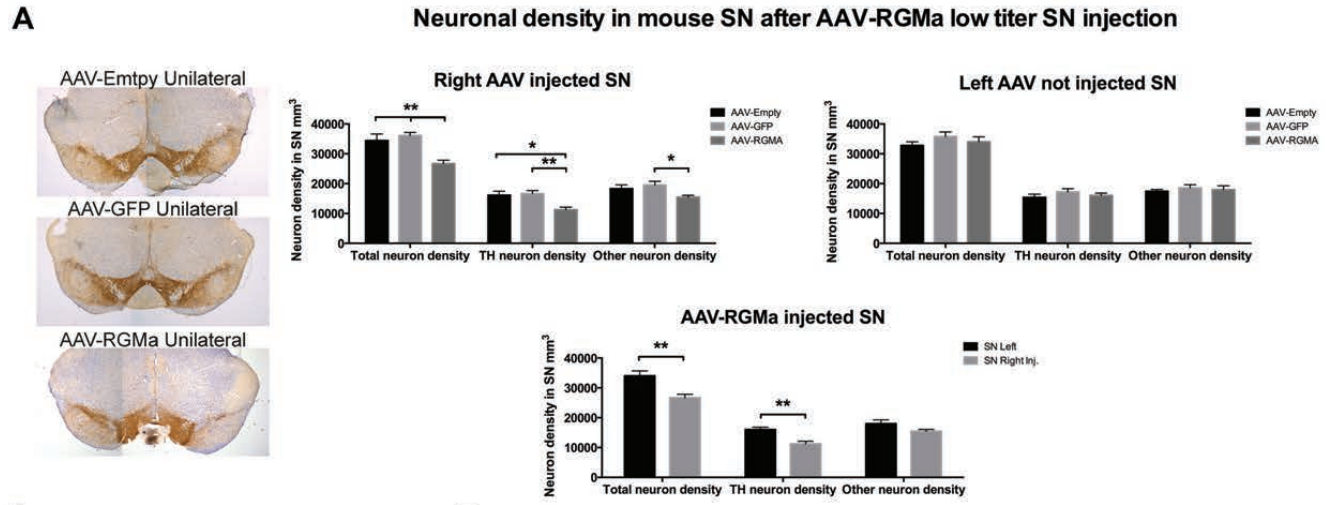

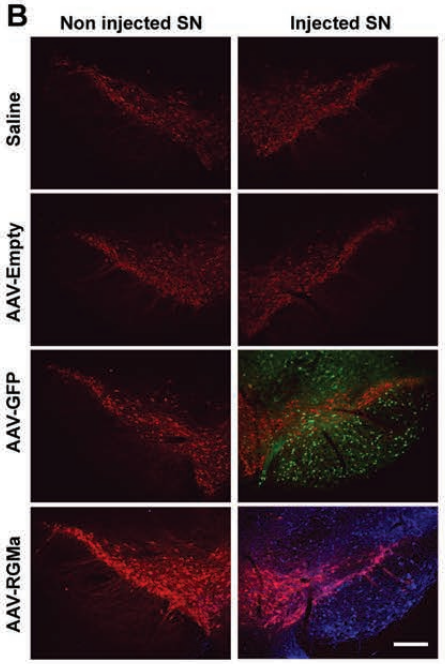

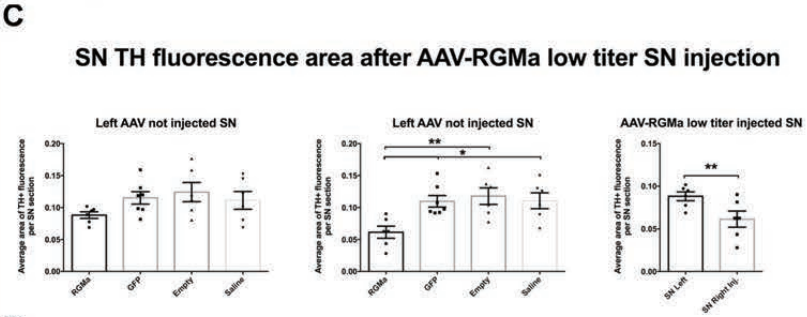

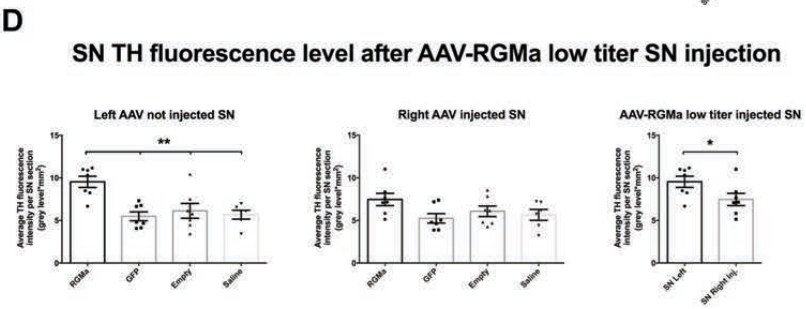

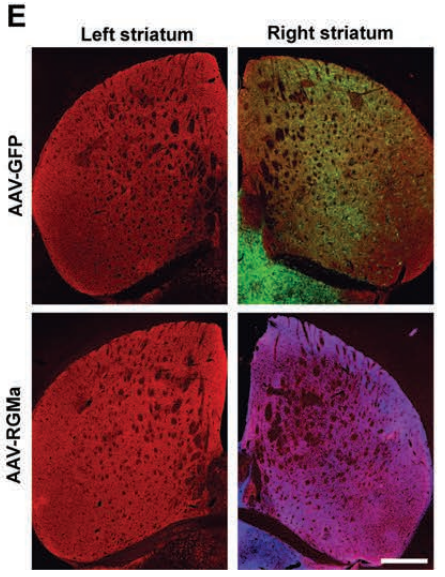

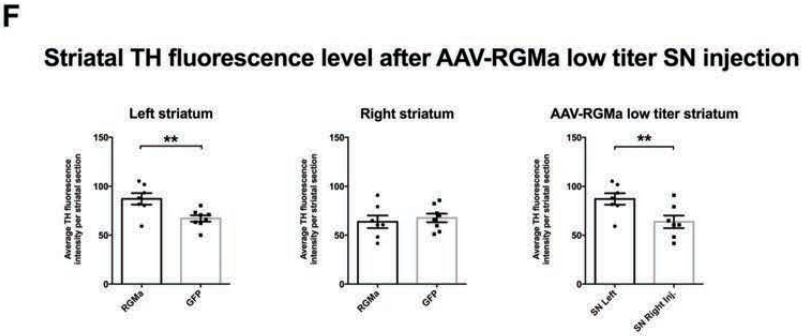

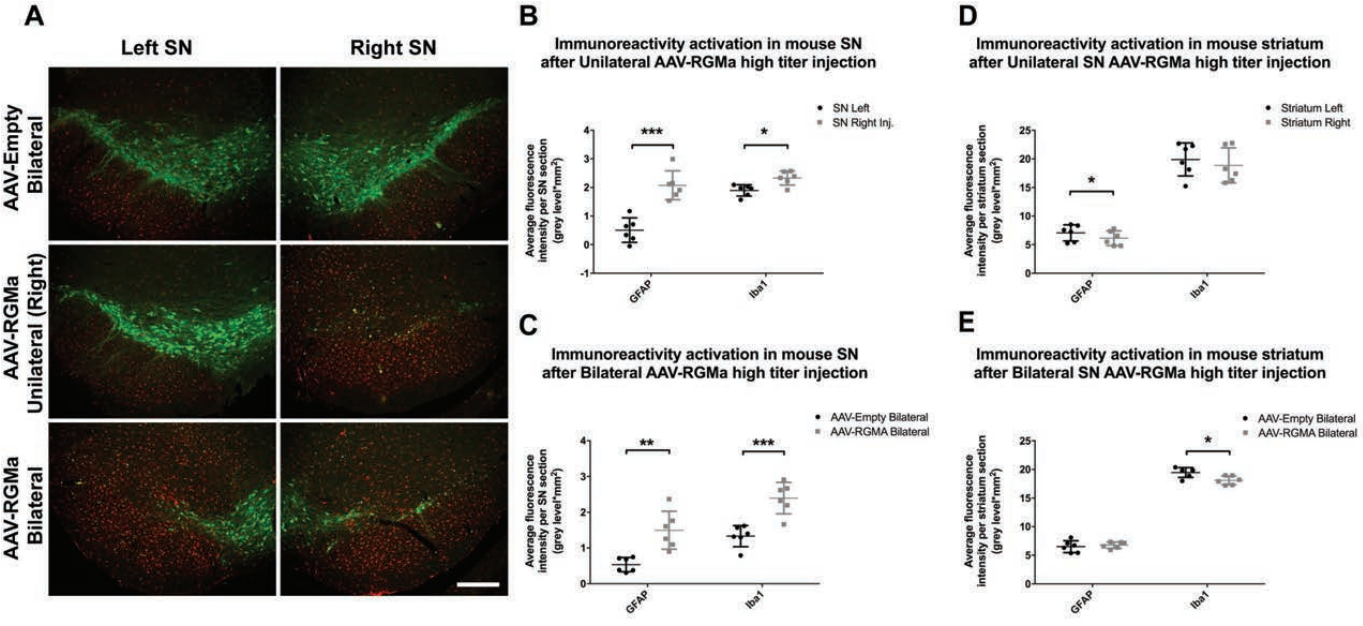

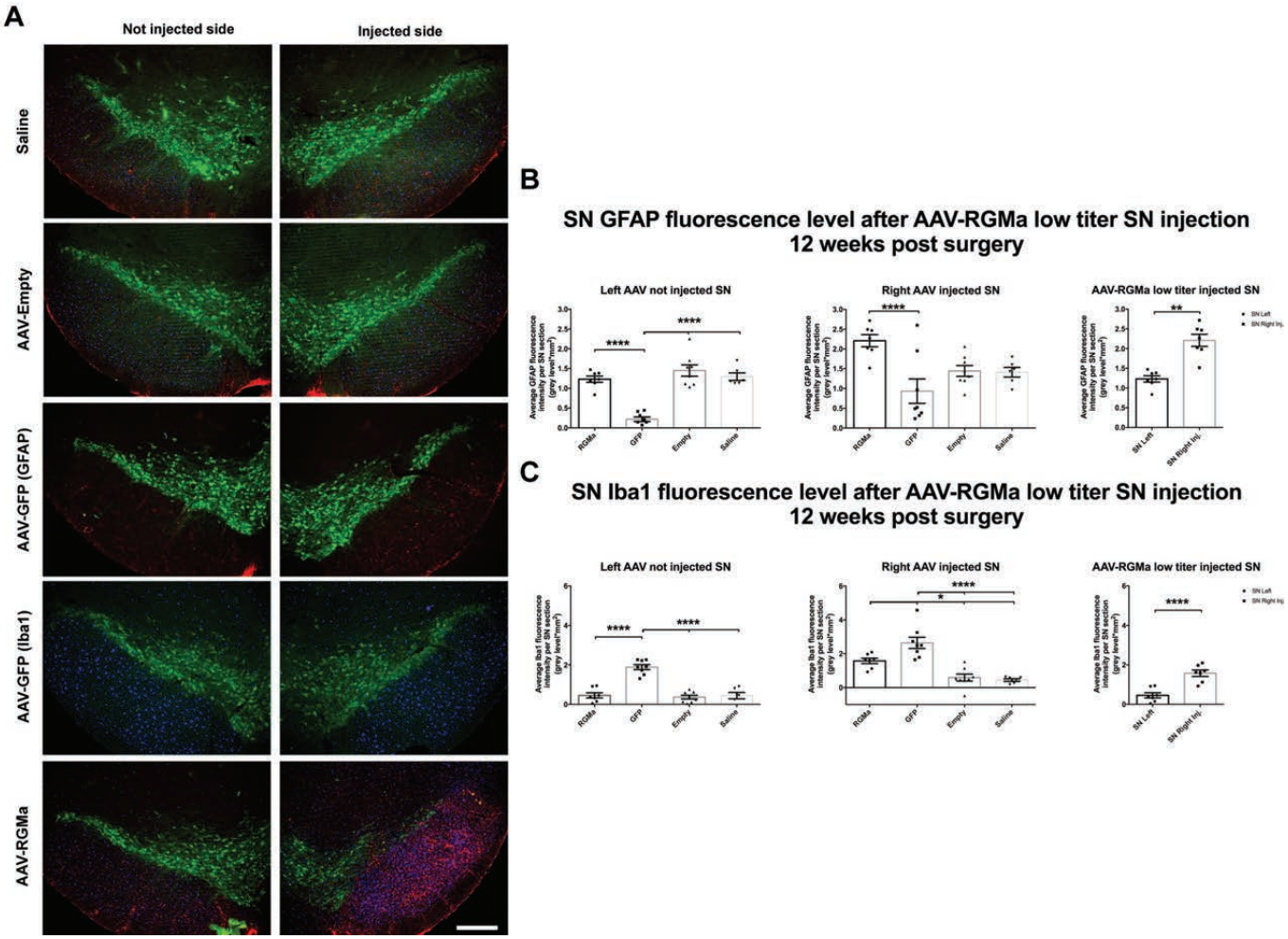

A

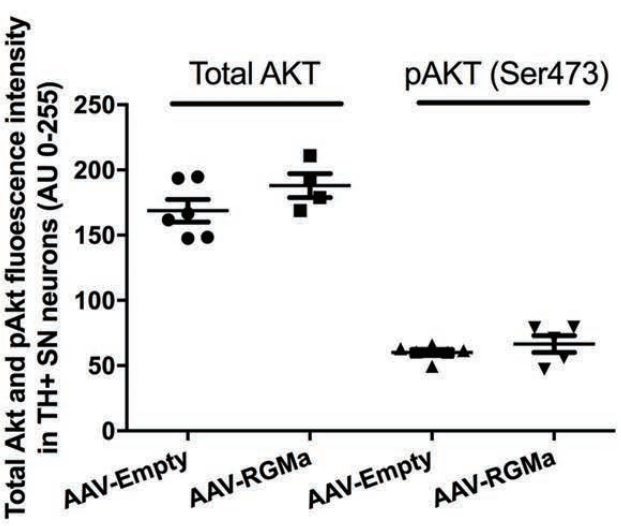

B